Nonlinear Dyn (2024) 112:9617–9637
https://doi.org/10.1007/s11071-024-09484-0

ORIGINAL PAPER

Stability and bifurcation analysis for a general nonlocal predator–prey system with top-hat kernel function

Xiaoxi Ding · **Yongli Song**

Received: 23 May 2023 / Accepted: 3 March 2024 / Published online: 5 April 2024

Abstract In this paper, we investigate the influence of the nonlocal intraspecific competition by the prey in a general predator–prey system on the stability and spatiotemporal dynamics, where the nonlocal kernel function is characterized by the top-hat function. It has been shown that when the nonlocal competition radius is sufficiently small, the nonlocal item has no impact on the stability of the spatially homogeneous steady state, but when the nonlocal competition radius is larger than some critical value, various types of spatiotemporal patterns occur via the bifurcation. The analytical conditions for the occurrence of Turing bifurcation, Hopf bifurcation and Turing–Hopf bifurcation are clearly determined. The spatially inhomogeneous steady states and inhomogeneous periodic patterns are found for the nonlocal Rosenzweig–MacArthur and Lotka–Volterra models with the top-hat kernel function.

Keywords Nonlocal intraspecific competition · Top-hat kernel · Stability · Bifurcation

Mathematics Subject Classification 35B32 · 35B35 · 92D25

X. Ding
Kharkiv Institute, Hangzhou Normal University, Hangzhou 311121, China

Y. Song (✉)
School of Mathematics, Hangzhou Normal University, Hangzhou 311121, China
e-mail: songyl@hznu.edu.cn

1 Introduction

Perception, usually referring to the ability of seeing, hearing or being conscious of something in other ways, is one of the important considerations that determine animal movement [8,33]. In some scenarios, this ability to perceive is assumed to be based on merely local information, which means that the intra-/inter-specific interactions only occur among/between individuals at the same spatial point. In a general sense, these are the so-called local behaviors. Furter and Grinfeld [9] originally overturned local hypothesis and novelly introduced nonlocal interactions in single-species population dynamics, and it has been shown that the nonlocal effect can lead to the spatial patterns even for the nonlocal kernel function characterized by the simple spatial average. Thereafter, many scholars are committed to studying the impact of nonlocal effect on the dynamics of the population dynamical models. The nonlocal term in the population models often appears as an integral form as follows

$$K * u = \int_{\Omega} K(x-y)u(y,t)dy, \tag{1.1}$$

where $u(y,t)$ is the population density at space y and time t, $K(x-y)$ is the some reasonable kernel function which measures the strength of the effect of a population at space y on a population at space x. For the finite domain Ω, if $K(x-y)$ is chosen as a constant function $K(x-y) = \frac{1}{|\Omega|}$, where $|\Omega|$ represents the volume of the domain Ω, then $K * u = \frac{1}{|\Omega|}\int_{\Omega} u(y,t)dy$ is the average value of u on the whole domain, denoted by $\bar{u} = \frac{1}{|\Omega|}\int_\Omega u(y,t)dy$, and the model including the term $\bar{u}$ is usually known as the model with the nonlocal spatial average [9]. The population model with the spatial average means that the growth of the population at the space x is related to the average value of the population on the whole space Ω. Recently, there has been an increasing activity and interest in the study of the dynamics of the population model with the spatial average. For instance, the existence and non-existence of positive solutions for the diffusive Lotka–Volterra system including nonlocal terms in the reaction functions has been investigated in [6]. The spatiotemporal patterns induced by the spatial average for the predator–prey model have been investigated in [7,10,11,15,20,37,39]. The joint effect of the spatial average and delay on the dynamics of the population models has been studied for a pollen tube model in [29] and for a predator–prey model in [31]. The stability, Turing bifurcation, Hopf bifurcation, Turing–Hopf bifurcation, double Hopf bifurcation and the corresponding normal form theory for the system with spatial average have been investigated in [5,25,34,35]. Especially, the detailed classification for Turing bifurcation and Hopf bifurcation induced by the spatial average in a general two variable reaction–diffusion system has been investigated in [28].

On the other hand, for an infinite domain or a periodic interval, the following top-hat kernel function (also known as the piece-wise constant kernel function) is often used in the literature [17,19,23]

$$K_M(z) = \begin{cases} \frac{1}{2M}, & |z| \le M, \\ 0, & |z| > M, \end{cases} \tag{1.2}$$

where $M \ge 0$ is often called the nonlocal competition radius of the prey (or known as the nonlocal perception radius in [33]), which means that the population can perceive resources within a fixed distance M from its current position, but resources beyond this fixed distance M will not be perceived, namely, the perception ability vanishes [33].

The influence of the top-hat function on the dynamics of the population models is also widely concerned by the biomathematicians. For instance, in [23], Bayliss and Volpert studied the complex predator invasion waves for the nonlocal Holling–Tanner model with the top-hat kernel function. In [3], Banerjee and Volpert investigated the existence of Turing patterns and the effect of the non-local interaction on the periodic travelling waves and spatio-temporal chaotic patterns in the nonlocal Rosenzweig–MacArthur model with the top-hat function. Patterns and various types of travelling waves due to the top-hat kernel function for the population models have been investigated by Genieys et al. [12]. Pattern formation in a three-species cyclic competition model with the top-hat kernel function has been numerically investigated in [16] and it has been shown that the introduction of nonlocality in intraspecific competitions stabilizes the system dynamics by transforming a dynamic population distribution to stationary. For more researches on the dynamics of the population models with the top-hat kernel function, see [2,4,18] and especially the review paper by Banerjee et al. [1] and the references therein.

However, most of the researches mentioned above on the dynamics of the nonlocal diffusive population models with the top-hat function rely heavily on specific models and numerical results. Theoretical work on more general nonlocal diffusive population models with the top-hat kernel function has not yet been done. Especially, there is little work on the Hopf bifurcation and Turing–Hopf bifurcation due to the nonlocality characterized by the top-hat kernel function.

In this paper, we start from the following general reaction–diffusion system

$$\begin{cases} N_\tau(x,\tau) = d_1 N_{xx}(x,\tau) + \widetilde{F}(N(x,\tau), P(x,\tau)), & x \in (-\infty,+\infty), \tau > 0, \\ P_\tau(x,\tau) = d_2 P_{xx}(x,\tau) + \widetilde{G}(N(x,\tau), P(x,\tau)), & x \in (-\infty,+\infty), \tau > 0, \end{cases} \tag{1.3}$$

where $N(x,\tau)$ and $P(x,\tau)$ are the densities of the prey and predator at location x and time τ, respectively, the reaction terms $\widetilde{F}$ and $\widetilde{G}$ describe the intra-/inter-species interaction among/between the individuals of the two species. Besides, the diffusion terms $d_1 N_{xx}(x,\tau)$ and $d_2 P_{xx}(x,\tau)$ represent the effect of random movement of the individuals within their habitat, d_1, d_2 are the diffusion coefficients. To reduce the diffusion coefficients, rescaling the time variable τ by $\tau = t/d_2$, and letting $u(x,t) = N(x,t/d_2)$, $v(x,t) = P(x,t/d_2)$, system (1.3) becomes

$$\begin{cases} u_t = d u_{xx} + F(u,v), & x \in (-\infty,+\infty), t > 0, \\ v_t = v_{xx} + G(u,v), & x \in (-\infty,+\infty), t > 0, \end{cases} \tag{1.4}$$

where

$$d = \frac{d_1}{d_2}, \ F(u,v) = \frac{\tilde{F}(N,P)}{d_2}, \ G(u,v) = \frac{\tilde{G}(N,P)}{d_2}.$$

In what follows, incorporating the nonlocal prey competition into model (1.4), we consider the following general nonlocal system with the top-hat kernel function:

$$\begin{cases} u_t = du_{xx} + F(u, K * u, v), & x \in (-\infty, +\infty), t > 0, \\ v_t = v_{xx} + G(u, v), & x \in (-\infty, +\infty), t > 0, \end{cases} \tag{1.5}$$

where

$$K * u = \int_{-\infty}^{+\infty} K_M(x-y)u(y,t)dy, \tag{1.6}$$

and $K_M(\cdot)$ is defined by (1.2). It will be seen in the following that when $M \to 0^+$, the nonlocal system (1.5) reduces to be a local system, which means the nonlocal competition radius M is the link between the local and nonlocal system. The main goal of this paper is to investigate analytically the influence of the nonlocal competition radius M on the stability and the possible bifurcation phenomena induced by the nonlocal term. And we also investigate the spatial patterns arising from the Turing bifurcation and spatially inhomogeneous oscillatory patterns arising from the Hopf bifurcation and Turing–Hopf bifurcation.

The paper is organized as follows. In Sect. 2, we investigate the stability and instability of the constant steady state and derive the analytical conditions for the existence of the bifurcations induced by nonlocal competition radius M. In Sect. 3, the obtained theoretical results are applied to the nonlocal diffusive Rosenzweig–MacArthur model and Lotka–Volterra model with top-hat kernel function to investigate the spatiotemporal dynamics. Spatial patterns and oscillatory patterns are shown via numerical simulations. Main results of this paper are summarized in the concluding Sect. 4. Throughout this paper, $\mathbb{N}$ represents the set of all positive integers and $\mathbb{N}_0 = \mathbb{N} \cup \{0\}$.

2 Stability and instability of spatially homogeneous steady state

Firstly, it follows from (1.2) and (2.2) that in the limiting case where $M \to 0^+$ (without nonlocal intraspecific perception), we have

$$\begin{aligned} \lim_{M\to 0^+} K_M * u &= \lim_{M\to 0^+} \int_{-\infty}^{+\infty} K_M(x-y)u(y,t)dy \\ &\xlongequal{\xi = x-y} \lim_{M\to 0^+} \int_{-\infty}^{+\infty} K_M(\xi)u(x-\xi,t)d\xi \\ &= \lim_{M\to 0^+} \int_{-M}^{M} \frac{1}{2M} u(x-\xi,t)d\xi \\ &\xlongequal{\exists \xi^* \in (-M,M)} \lim_{\xi^*\to 0^+} u(x-\xi^*,t) = u(x,t), \end{aligned} \tag{2.1}$$

which means that the nonlocal term reduces to be local term as $M \to 0^+$. The local system corresponding to the nonlocal perceptual system (1.5) is

$$\begin{cases} u_t = du_{xx} + F(u, u, v), & x \in (-\infty, +\infty), \ t > 0, \\ v_t = v_{xx} + G(u, v), & x \in (-\infty, +\infty), \ t > 0. \end{cases} \tag{2.2}$$

Suppose that there are two positive numbers u_* and v_* satisfying $F(u_*, u_*, v_*) = G(u_*, v_*) = 0$, which means $E_* = (u_*, v_*)$ is the positive constant steady state of system (2.2).

Throughout this paper, what we call the stability of E_* means the stability given by the following definition.

Definition 2.1 For $\forall \epsilon > 0$, $\exists \delta > 0$ and $T > 0$, when $||(u(x,0), v(x,0)) - (u_*, v_*))||_2 < \delta$, we have $||(u(x,t), v(x,t)) - (u_*, v_*))||_2 < \epsilon$ for $t > T$. Here $|| \cdot ||_2$ is the usual L_2 norm.

In what follows, we always assume that E_* of system (2.2) is locally asymptotically stable, i.e., the following conditions (C_0) and (C_1) hold

$$a_1 + a_4 < 0, \ \ a_1a_4 - a_2a_3 > 0, \tag{C_0}$$

and

$$a_1 + a_4 d < 2\sqrt{d(a_1a_4 - a_2a_3)}, \tag{C_1}$$

where

$$\begin{aligned} a_1 &= \left.\frac{\partial F(u,u,v)}{\partial u}\right|_{(u_*,u_*,v_*)}, \ a_2 = \left.\frac{\partial F(u,u,v)}{\partial v}\right|_{(u_*,u_*,v_*)}, \\ a_3 &= \left.\frac{\partial G(u,v)}{\partial u}\right|_{(u_*,v_*)}, \quad a_4 = \left.\frac{\partial G(u,v)}{\partial v}\right|_{(u_*,v_*)}. \end{aligned} \tag{2.3}$$

The condition (C_0) implies that E_* as the equilibrium of the corresponding ordinary differential equations (ODE) of (2.2) is asymptotically stable and the condition (C_1) implies that there is no diffusion-driven Turing instability for (2.2). This means that without nonlocal perception (i.e., $M = 0$), E_* is always asymptotically stable. Noticing that $K * u_* = u_*$ from (1.6), E_* is also the positive equilibrium of system (1.5).

In the following, we investigate the influence of nonlocal competition radius $M > 0$ on the stability of the equilibrium E_* of the system (1.5) and the possible bifurcation phenomena in which the nonlocal term plays a decisive role.

The linearized system of (1.5) at E_* is

$$\begin{pmatrix} u_t \\ v_t \end{pmatrix} = D\begin{pmatrix} u_{xx} \\ v_{xx} \end{pmatrix} + A_1\begin{pmatrix} u \\ v \end{pmatrix} + A_2\begin{pmatrix} K*u \\ 0 \end{pmatrix}, \tag{2.4}$$

where

$$D = \begin{pmatrix} d & 0 \\ 0 & 1 \end{pmatrix},\ A_1 = \begin{pmatrix} a_{11} & a_2 \\ a_3 & a_4 \end{pmatrix}, \quad A_2 = \begin{pmatrix} a_{12} & 0 \\ 0 & 0 \end{pmatrix}, \tag{2.5}$$

with

$$a_{11} = \left.\frac{\partial F(u, K*u, v)}{\partial u}\right|_{(u_*,u_*,v_*)}, \quad a_{12} = \left.\frac{\partial F(u, K*u, v)}{\partial (K*u)}\right|_{(u_*,u_*,v_*)}. \tag{2.6}$$

From (2.3) and (2.6), it is easy to see that $a_1 = a_{11}+a_{12}$, which will be used in the following analysis. From a biological point of view, in the following analysis, we also assume the following condition

$$a_2 < 0,\ a_3 > 0,\ a_{12} < 0, a_4 \le 0 \tag{C_2}$$

holds. The assumptions $a_2 < 0, a_3 > 0$ imply that u is the prey and v is the predator and the assumption $a_{12} < 0$ implies that the nonlocal effect arises from the intraspecific competition. The assumption $a_4 \le 0$ often appears in many predator–prey systems [2,14,36,38,40].

Then we assume that the solution of (2.4) is in form of

$$\begin{pmatrix} u(x,t) \\ v(x,t) \end{pmatrix} = \begin{pmatrix} a_k \\ b_k \end{pmatrix} e^{\lambda t + ikx}, \tag{2.7}$$

where $\lambda \in \mathbb{C}$, $k \in \mathbb{R}$. For the nonlocal item $K*u$, we have

$$\begin{aligned} K*u &= \int_{-\infty}^{+\infty} K(x-y) a_k e^{\lambda t + iky} dy \\ &= a_k e^{\lambda t}\int_{-\infty}^{+\infty} K(z) e^{ik(x-z)} dz \\ &= a_k e^{\lambda t + ikx}\int_{-\infty}^{+\infty} K(z) e^{-ikz} dz = uH(k,M), \end{aligned} \tag{2.8}$$

where

$$\begin{aligned} H(k,M) &= \int_{-\infty}^{+\infty} K(z)\, e^{-ikz} dz = \frac{1}{2M}\int_{-M}^{M} e^{-ikz} dz \\ &= \begin{cases} \frac{\sin(kM)}{kM}, & k \ne 0, \\ 1, & k = 0. \end{cases} \end{aligned} \tag{2.9}$$

Then, substituting (2.7) into (2.4), we obtain the following characteristic equation

$$\Gamma_k(\lambda) \overset{def}{=\!=} \lambda^2 - T(k,M)\lambda + J(k,M) = 0, \tag{2.10}$$

in which

$$\begin{aligned} T(k,M) &= Tr(A_1) + a_{12}H(k,M) - Tr(D)k^2, \\ J(k,M) &= dk^4 - (a_{12}H(k,M) + a_{11} + da_4)k^2 \\ &\quad + a_{12}a_4 H(k,M) + Det(A_1). \end{aligned} \tag{2.11}$$

From (2.9) and (2.11), for $k = 0$, we have $H(0,M) = 1$ for any $M \ge 0$, then Eq. (2.10) becomes

$$\lambda^2 - (a_1 + a_4)\lambda + (a_1 a_4 - a_2 a_3) = 0, \tag{2.12}$$

which is the characteristic equation of corresponding ODE of system (1.5) at E_*. Under the condition (C_0), two roots of Eq. (2.12) have negative real parts.

For $M = 0$, we have $H(k,0) = 1$ for $k \ne 0$ and $k \in \mathbb{R}$, Then Eq. (2.10) becomes

$$\lambda^2 - \left(a_1 + a_4 - Tr(D)k^2\right)\lambda + (dk^4 - (a_1 + da_4)k^2 + a_1 a_4 - a_2 a_3) = 0, \tag{2.13}$$

which is the characteristic equation of system (2.2) at E_*, which does not include the nonlocal term. Under the condition (C_1), two roots of Eq. (2.13) have negative real parts.

Obviously, $T(k,M)$ and $J(k,M)$ are even functions with respect to k. Thus we only need to consider the case of $k > 0$. In what follows, we focus on the case of $k > 0$ and $M > 0$ and investigate the distribution of roots of the characteristic equation (2.10). Notice that the change of the stability of the steady state E_* and the bifurcation is related to the characteristic roots with zero real parts, and different perception radius M can be chosen to change the value of $H(k,M)$ such that $T(k,M) = 0$ or $J(k,M) = 0$. Therefore, the perception radius M can affect the stability of the steady state E_* of system (1.5) and the possible bifurcation phenomena will occur. More specifically, the steady state E_* can lose its stability through the following bifurcations if there exist $k_* \ne 0$ and $M_* \ne 0$ such that

$T(k,M) < 0$ for $k, M > 0$, $J(k,M)$

$$\begin{cases} = 0, & k = k_*, M = M_*, \\ > 0, & k \neq k_*, M \neq M_*, \end{cases} \tag{2.14}$$

which is related to the Turing bifurcation, and

$$J(k, M) > 0 \text{ for } k, M > 0, \ T(k, M)$$
$$\begin{cases} = 0, & k = k_*, M = M_*, \\ < 0, & k \neq k_*, M \neq M_*, \end{cases} \tag{2.15}$$

which is related to the spatially inhomogeneous Hopf bifurcation with spatial mode-k_*.

From (2.11), it is easy to verify that $T(k, M) < 0$ is equivalent to

$$-a_{12} H(k, M) > -(d+1)k^2 + a_{11} + a_4, \tag{2.16}$$

and $J(k, M) > 0$ is equivalent to

$$-a_{12} H(k, M) > -d(k^2 - a_4) + \frac{a_2 a_3}{k^2 - a_4} + a_{11} - d a_4. \tag{2.17}$$

Let

$$h(k, d) = -\frac{(d+1)k^2}{a_{12}} + \frac{a_{11} + a_4}{a_{12}}, \tag{2.18}$$

$$f(k, d) = -\frac{d\left(k^2 - a_4\right)}{a_{12}} + \frac{a_2 a_3}{a_{12}\left(k^2 - a_4\right)} + \frac{a_{11} - d a_4}{a_{12}}, \tag{2.19}$$

$$g(k, M) = -\frac{\sin(kM)}{kM}. \tag{2.20}$$

Noticing $g(k, M) = -H(k, M)$ for $k \neq 0$ and then by (2.11), (2.18), and (2.19), we have

$$\begin{aligned} T(k, M) &= a_{12}\left(h(k, d) - g(k, M)\right), \\ &= J(k, M) = a_{12}\left(g(k, M) - f(k, d)\right). \end{aligned}$$

Considering $a_{12} < 0$, then, for $k > 0$, $T(k, M) < 0$ if and only if $g(k, M) < h(k, d)$ by (2.16) and $J(k, M) > 0$ if and only if $g(k, M) < f(k, d)$ by (2.17). The properties of the function $g(k, M)$ are very useful in the following analysis.

For (2.20), substituting $z = kM$, we denote $g_1(z) \stackrel{\Delta}{=} -\frac{\sin(z)}{z}$. Denoting the countable number of positive roots of the equation $\tan(z) = z$ by $z_j > 0$, we have the following preliminary properties with regard to $g(k, M)$, whose proof is simple and similar to Proposition 3.1 in [32]. So, we omit it here.

Proposition 2.2 *For fixed M, we have*

(i) *$g(k, M)$ obtains its local maximum at $k = k_j \stackrel{\Delta}{=} \frac{z_j}{M}$, $j = 2(m-1)+1$, and*
$$g\left(k_{(2m-1)}, M\right) > g\left(k_{(2m+1)}, M\right) > 0, \ m \in \mathbb{N};$$

(ii) *$g(k, M)$ obtains its local minimum at $k = k_j \stackrel{\Delta}{=} \frac{z_j}{M}$, $j = 2m$, and*
$$g\left(k_{2m}, M\right) < g\left(k_{2(m+1)}, M\right) < 0, \ m \in \mathbb{N}.$$

By Proposition 2.2, it is easy to see that the oscillating function $g(k, M)$ fluctuates up and down along the k axis and obtain its maximum $-\sin(z_1)/z_1$ at $k_1 = \frac{z_1}{M}$. Obviously, $g\left(\frac{n\pi}{M}, M\right) = 0$ $(n \in \mathbb{N})$ and $g(k, M) < 0$ for $0 < k < \frac{\pi}{M}$. Notice that

$$\lim_{M \to 0^+} k_1 = +\infty, \quad \lim_{M \to +\infty} k_1 = 0. \tag{2.21}$$

Therefore, when M varies from small to large, the maximum $-\sin(z_1)/z_1$ of $g = g(k, M)$ keeps the same and the maximum point moves from right to left along the straight line $g = -\sin(z_1)/z_1$, as shown in Fig. 1.

With the choice of these parameters as shown in Fig. 1, the real part of the eigenvalue of linear operator will be shown in Fig. 3. For $M < M_1^c$, all roots of Eq. (2.10) have negative real parts as shown in Fig. 3a. For $M = M_1^c$, Eq. (2.10) has a zero root when $M = M_1^c$, $k = k_1^c$ as shown in Fig. 3d. For $M > M_1^c$, there exist some k such that Eq. (2.10) has positive real roots or one pair of complex roots with positive real parts as shown in Fig. 3g–i.

Furthermore, by calculating the equation $\tan(z_j) = z_j$, $j \in \mathbb{N}$, we have $z_1 = 4.4934$ and the maximum of $g(k, M)$ is $-\sin(z_1)/z_1 \doteq 0.2172$. For the convenience of notation, we denote

$$\beta = -z_1/\sin(z_1) \doteq 4.6033. \tag{2.22}$$

We firstly investigate the influence of M on the sign of $T(k, M)$. For fixed d, $h(k, d)$ is a function with respect to k, which is independent of M. However, based on the proposition 2.2 and (2.21), $g(k, M)$ is an oscillating function of M and k, moving from right to left along k axis when M varies from small to large. Therefore, it is easy to see that there exists the critical value M_H of M and the critical value K_H of k such that

$$\begin{aligned} & g(k_H, M_H) = h(k_H, d), \\ & \frac{\partial g(k_H, M_H)}{\partial k} = \frac{\partial h(k_H, d)}{\partial k}, \end{aligned} \tag{2.23}$$

with $0 < k_H M_H < z_1$, i.e., the curve $g = g(k, M_H)$ is tangent to the curve $h = h(k, d)$ at $k = k_H$. Then we have the following results on the sign of $T(k, M)$.

Lemma 2.3 *Assume that the conditions (C_0), (C_1) and (C_2) hold, β and M_H are defined by (2.22) and (2.23). Then we have the following results:*

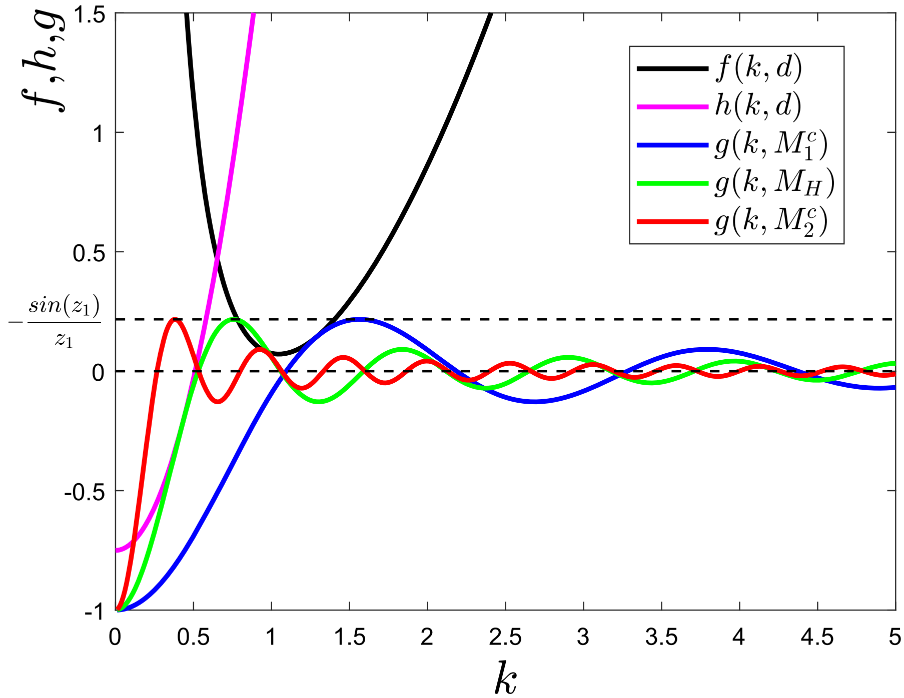

Fig. 1 The curves $f = f(k, d)$ and $h = h(k, d)$ are independent of M with $d = 0.15$, $a_{11} = 0.3$, $a_{12} = -0.4$, $a_2 = -0.6$, $a_3 = 0.3$, $a_4 = 0$, and the oscillating curves $g = (k, M)$ move from right to left along the k axis with increasing of M, making the tangency at the critical values $M_1^c = 2.8740$, $M_H = 5.9316$, $M_2^c = 11.7948$ of M. In terms of the equation $\tan(z_j) = z_j$, we have $z_1 = 4.4934$ and the maximum of $g(k, M)$ is $-\frac{\sin(z_1)}{(z_1)} = 0.2172$

(I) *if* $a_{12} \geq \beta(a_{11} + a_4)$, *then* $T(k, M) < 0$ *for any* $k > 0$ *and* $M > 0$*;*

(II) *if* $a_{12} < \beta(a_{11} + a_4)$*, then we have the following results:*

  (i) *for* $0 < M < M_H$*,* $T(k, M) < 0$ *for* $k > 0$*;*

  (ii) *for* $M = M_H$*,* $T(k_H, M_H) = 0$ *and* $T(k, M_H) < 0$ *for* $k \neq k_H$*;*

  (iii) *for* $M > M_H$*, then* $\exists\ I_k \subset \mathbb{R}^+$ *such that* $T(k, M) > 0$ *for* $k \in I_k$ *and* $T(k, M) \leq 0$ *for* $k \notin I_k$*.*

Proof When $a_{12} < 0$, it follows from (2.16) that $T(k, M) < 0$ if and only if $g(k, M) < h(k, d)$ for any $k > 0$. Thus we compare the $\max\limits_{k>0}\{g(k, M)\}$ with $\min\limits_{k>0}\{h(k, d)\}$. By Proposition 2.2, it is easy to see that

$$\max_{k>0}\{g(k, M)\} = \max_{z>0}\{g_1(z)\} = -\frac{\sin z_1}{z_1} > 0, \quad (2.24)$$

in which $z_1 \in (\pi, 3\pi/2)$. From (2.18), for fixed $d > 0$, $h(k, d)$ is a parabolic function with respect to k and since $a_{12} < 0$, we have

$$\frac{\partial h(k, d)}{\partial k} = -\frac{2(d + 1)k}{a_{12}} > 0, \quad (2.25)$$

which implies that $h(k, d)$ is increasing for $k > 0$. Obviously, together with (C_0), we have

$$\min_{k>0}\{h(k, d)\} > h(0, d) = \frac{a_{11} + a_4}{a_{12}} > -1.$$

When $a_{12} \geq \beta(a_{11} + a_4)$, namely $a_{11} + a_4 \leq -\frac{\sin z_1}{z_1} a_{12}$, it is easy to verify that

$$\begin{aligned}\min_{k>0}\{h(k, d)\} &> \frac{a_{11} + a_4}{a_{12}} \\ &\geq -\frac{\sin(z_1)}{z_1} \geq \max_{k\geq 0}\{g(k, M)\},\end{aligned} \quad (2.26)$$

thus we have $h(k, d) > g(k, M)$, which means $T(k, M) < 0$ for any $k > 0$ and $M > 0$. The conclusion (I) is confirmed.

When $a_{12} < \beta(a_{11} + a_4)$, which is equivalent to $a_{11} + a_4 > -\frac{\sin z_1}{z_1} a_{12}$, we have $-1 < \min\limits_{k>0}\{h(k, d)\} < -\frac{\sin(z_1)}{z_1}$. From proposition 2.2, we have the fact that $g(k, M)$ is an oscillating function of M and k. When M varies from small to large, $g(k, M)$ moves from right to left along k axis. Notice that (2.21), when M is sufficiently small, the maximum value of $g(k, M)$ can be obtained when k is large enough. In addition,

$$\lim_{k\to+\infty} h(k, d) = +\infty,$$
$$\lim_{k\to+\infty} g(k, M) = 0.$$

Hence when M is sufficiently small, we have $g(k, M) < h(k, d)$ for any $k > 0$, i.e., $T(k, M) < 0$ for any $k > 0$.

When M varies from small to large to M_H, the curve $g = g(k, M_H)$ is tangent to the curve $h = h(k, d)$ at $k = k_H$ and $h(k, d) > g(k, M_H)$ for $k \neq k_H$, i.e., $T(k_H, M_H) = 0$, and $T(k, M_H) < 0$ for $k \neq k_H$.

With the increasing of M, the curve $g = g(k, M)$ moves from right to left and cross the curve $h = h(k, d)$. Thus for $M > M_H$, there exist a small interval $I_k \subset \mathbb{R}^+$ such that for $k \in I_k$, we have $h(k, d) < g(k, M)$, i.e., $T(k, M) > 0$ and for $k \notin I_k$, $T(k, M) < 0$. The conclusion (II) is confirmed. □

Then we investigate the influence of M on the sign of $J(k, M)$. Notice that (2.17), we have $J(k, M) > 0$ if and only if $g(k, M) < f(k, d)$ for any $k > 0$. As such, we compare the $\max_{k>0}\{g(k, M)\}$ with $\min_{k>0}\{f(k, d)\}$. We firstly give the following results on the relation between the minimum of the curve $f = f(k, d)$ and the local extremum $g_1(z_m)$ of the curve $g = g_1(z)$, which can determine the sign of $J(k, M)$.

Lemma 2.4 *Assume that the conditions (C_0), (C_1) and (C_2) hold. Denoting the solution of $\min_{k>0} f(k, d) = g_1(z_m)$ by $d^{(m)}$, $m \in \mathbb{N}$, then*

(i) *for $a_4 = 0$, we have*

$$d^{(m)} = \frac{\left(a_{11} + \frac{\sin(z_m)}{z_m} a_{12}\right)^2}{-4a_2a_3} \tag{2.27}$$

provided that

$$a_{11} + \frac{\sin(z_m)}{z_m} a_{12} > 0;$$

(ii) *for $a_4 < 0$, we have*

$$d_-^{(m)} = \frac{1}{a_4^2}\left(\sqrt{\left(a_{11} + \frac{\sin(z_m)}{z_m} a_{12}\right) a_4 - a_2a_3} - \sqrt{-a_2a_3}\right)^2 \tag{2.28}$$

provided that

$$0 < a_{11} + \frac{\sin(z_m)}{z_m} a_{12} < \frac{a_2a_3}{a_4}.$$

Proof From (2.19), for $a_4 = 0$, we have $f(k, d)$ is an even function with respect to k and

$$\frac{\partial f(k, d)}{\partial k} = -\frac{2dk}{a_{12}} - \frac{2a_2a_3}{a_{12}k^3},$$

which, implies that for fixed $d > 0$, $f(k, d)$ is increasing for $0 < k < k_c$ and decreasing for $k > k_c$, where $k_c = \sqrt[4]{\frac{-a_2a_3}{d}}$. Note the fact that $a_1 = a_{11} + a_{12}$ and $a_{12} < 0$. Hence, together with (C_0), it is easy to conclude that

$$\min_{k>0}\{f(k, d)\} = f(k_c, d)$$
$$= \frac{a_{11} - 2\sqrt{-a_2a_3d}}{a_{12}} > \frac{a_{11}}{a_{12}} > -1. \tag{2.29}$$

Thus by $\min_{k>0} f(k, d) = g_1(z_m)$, $m \in \mathbb{N}$, we obtain

$$a_{11} + \frac{\sin(z_m)}{z_m} a_{12} = 2\sqrt{-a_2a_3d},$$

which means that $d^{(m)}$ exists if and only if $a_{11} + \frac{\sin(z_m)}{z_m} a_{12} > 0$. The conclusion (i) is proved.

In addition, for $a_4 < 0$, it is easy to verify that

$$\min_{k>0}\{f(k, d)\} = \begin{cases} \frac{a_{11} - da_4 - 2\sqrt{-da_2a_3}}{a_{12}}, & 0 \le d < \frac{-a_2a_3}{a_4^2}, \\ \frac{a_{11}a_4 - a_2a_3}{a_{12}a_4}, & d \ge \frac{-a_2a_3}{a_4^2}, \end{cases} \tag{2.30}$$

then the conclusion (ii) follows immediately by solving $\min_{k>0} f(k, d) = g_1(z_m)$ for d. □

By calculating $\min_{k>0} f(k, d) = 0$, for $a_4 = 0$, we have

$$\tilde{d} = \frac{a_{11}^2}{-4a_2a_3}, \tag{2.31}$$

provided that $a_{11} > 0$. For $a_4 < 0$, we have

$$\tilde{d}_- = \frac{1}{a_4^2}\left(\sqrt{a_{11}a_4 - a_2a_3} - \sqrt{-a_2a_3}\right)^2, \tag{2.32}$$

provided that $0 < a_{11} < \frac{a_2a_3}{a_4}$, which both are the critical values of d to determine the sign of minimum of the curve $f = f(k, d)$ for the cases of $a_4 = 0$ and $a_4 < 0$, respectively.

According to Lemma 2.4, the minimum value of the function $f(k, d)$ differs when $a_4 = 0$ and $a_4 < 0$, which has a direct influence on the sign of $J(k, M)$, further leading to different conditions for the stability of the steady state E_* and the possible bifurcation phenomena. Thus, the following investigations are divided into two cases: $a_4 = 0$ and $a_4 < 0$.

2.1 Stability and bifurcations for the case of $a_4 = 0$

In this subsection, we mainly investigate the influence of the nonlocal competition radius M on the stability of the steady state E_* and the possible bifurcation phenomena for the case of $a_4 = 0$.

We make further efforts to investigate the influence of the diffusion coefficient d and the competition radius M on the sign of $J(k, M)$. For fixed d, $f(k, d)$ is a function with respect to k, which is independent of M. However, on account of proposition 2.2 and (2.21), we have $g(k, M)$ is an oscillating function of M and k, moving from right to left along k axis when M varies from small to large. Then we have the following results.

When $a_{12} \geq \beta a_{11}$, we can obtain that $\min\limits_{k>0}\{f(k, d)\}$ is always larger than $\max\limits_{k>0}\{g(k, M)\}$ no matter what value M takes, that is, we have the following lemma.

Lemma 2.5 *Assume that the conditions* (C_0), (C_1) *and* (C_2) *hold. For* $a_{12} \geq \beta a_{11}$, *we have* $J(k, M) > 0$ *for any* $M > 0$ *and* $k > 0$.

Proof When $a_{12} \geq \beta a_{11}$, from (2.29) and (2.24), we have $\min\limits_{k>0}\{f(k, d)\} > \frac{a_{11}}{a_{12}} \geq -\frac{\sin(z_1)}{z_1} \geq \max\limits_{k>0}\{g(k, M)\}$, i.e., $J(k, M) > 0$ for any $M > 0$ and $k > 0$. □

When $a_{12} < \beta a_{11}$, notice that the joint action of d and M determines the sign of $J(k, M)$, so that $\min\limits_{k>0}\{f(k, d)\}$ is less than $\max\limits_{k>0}\{g(k, M)\}$. For $a_{11} \leq 0$, it follows from (2.29) that $\min\limits_{k>0}\{f(k, d)\} > 0$. Then combined with Lemma 2.4, when M varies from small to large, there exist the values M_{T_i} of M and k_{T_i} of k $(i \in \mathbb{N})$ such that

$$\begin{aligned} &g(k_{T_i}, M_{T_i}) = f(k_{T_i}, d), \\ &\frac{\partial}{\partial k} g(k_{T_i}, M_{T_i}) = \frac{\partial}{\partial k} f(k_{T_i}, d). \end{aligned} \tag{2.33}$$

Letting

$$M_1^c = \min_{i\in\mathbb{N}}\{M_{T_i}\}, \quad M_2^c = \max_{i\in\mathbb{N}}\{M_{T_i}\}, \tag{2.34}$$

we have $M_1^c = M_{T_1} < M_{T_2} < \cdots \leq M_2^c$, which means for $M = M_1^c$ and $M = M_2^c$, the curve $g = g(k, M)$ is firstly and lastly tangent to the curve $f = f(k, d)$ at $k = k_1^c$ and $k = k_2^c$ respectively. We define

$$\begin{aligned} I_M = \big\{M \in \big(M_1^c, M_2^c\big) \\ |f(k, d) < g(k, M) \text{ for some } k > 0\big\}. \end{aligned} \tag{2.35}$$

Obviously, it follows from (2.33) and (2.34) that there exists some $k > 0$ resulting in $f(k, d) < g(k, M)$ when M is larger than and sufficiently close to M_1^c or M is smaller than and close enough to M_2^c. As such, the set I_M defined by (2.35) is not empty.

Then we obtain the following results:

Lemma 2.6 *Assume that the conditions* (C_0), (C_1) *and* (C_2) *hold,* $d^{(1)}$, I_M, M_1^c *and* M_2^c *are defined by* (2.27), (2.35) *and* (2.34), *respectively. For* $a_{12} < \beta a_{11} \leq 0$, *we obtain the following results:*

(I) *if* $d > d^{(1)}$, $J(k, M) > 0$ *for any* $M > 0$ *and* $k > 0$;
(II) *if* $d = d^{(1)}$, $J(k_c, \frac{z_1}{k_c}) = 0$ *and* $J(k, M) > 0$ *for* $M \neq \frac{z_1}{k_c}$ *where* $k_c = \sqrt[4]{\frac{-a_2 a_3}{d}}$;
(III) *if* $0 < d < d^{(1)}$, *then there exist two critical values* M_1^c *and* M_2^c *of* M *such that*
  (i) *for* $M \in (0, M_1^c) \cup (M_2^c, +\infty)$, $J(k, M) > 0$ *for* $k > 0$;
  (ii) *for* $M = M_j^c$, $J(k_j^c, M_j^c) = 0$ *and* $J(k, M_j^c) > 0$ *for* $k \neq k_j^c (j = 1, 2)$;
  (iii) *for* $M \in (M_1^c, M_2^c)$, *the sign of* $J(k, M)$ *depends on the values of* M. *More specifically, for* $M \in I_M$, *there exists at least one* $k > 0$ *such that* $J(k, M) < 0$; *for* $M \in (M_1^c, M_2^c) \setminus I_M$, *then* $J(k, M) > 0$ *for any* $k > 0$.

Proof When $a_{12} < \beta a_{11}$, i.e., $a_{11} > -\frac{\sin(z_1)}{z_1} a_{12}$, note that the minimum value of $f(k, d)$ and the maximum value of $g(k, M)$ are independent of M. It follows from (2.27) and (2.29) and (2.24) that for $d > d^{(1)}$, we have

$$\min_{k>0}\{f(k, d)\} > \max_{k>0}\{g(k, M)\},$$

so $f(k, d) > g(k, M)$ for any $k > 0$ and $M \geq 0$, i.e., $J(k, M) > 0$ for any $k > 0$ and $M > 0$. The conclusion (I) is confirmed.

For $d = d^{(1)}$, we have $\min\limits_{k>0}\{f(k, d)\} = f(k_c, d^{(1)}) = \frac{a_{11} - 2\sqrt{-a_2 a_3 d^{(1)}}}{a_{12}} = -\frac{\sin(z_1)}{z_1}$, where $k_c = \sqrt[4]{\frac{-a_2 a_3}{d}}$. Thus we have $f(k_c, d) = g(k_c, \frac{z_1}{k_c})$, i.e., $J(k_c, \frac{z_1}{k_c}) = 0$ and $J(k, M) > 0$ for $M \neq \frac{z_1}{k_c}$. The conclusion (II) is confirmed.

For $0 < d < d^{(1)}$, notice that (2.21) and

$$\lim_{k\to+\infty} f(k, d) = +\infty, \lim_{k\to+\infty} g(k, M) = 0.$$

Therefor when M is sufficiently small $(M < M_1^c)$, we have $g(k, M) < f(k, d)$ for any $k > 0$, i.e., $J(k, M) > 0$ for any $k > 0$.

When M varies from small to large to M_1^c, the curve $g = g(k, M_1^c)$ is firstly tangent to the curve $f = f(k, d)$ at $k = k_1^c$ and $f(k, d) > g(k, M_1^c)$ for

$k \neq k_1^c$, i.e., $J(k_1^c, M_1^c) = 0$, and $J(k, M_1^c) > 0$ for $k \neq k_1^c$.

With the increasing of M, the curve $g = g(k, M)$ moves from right to left and crosses the curve $f = f(k, d)$. When M increases to $M = M_2^c$, the curve $g = g(k, M_2^c)$ is lastly tangent to the curve $f = f(k, d)$ at $k = k_2^c$ and $f(k, d) > g(k, M_2^c)$ for $k \neq k_2^c$, i.e., $J(k_2^c, M_2^c) = 0$, and $J(k, M_2^c) > 0$ for $k \neq k_2^c$.

Then for $M \in \left(M_1^c, M_2^c\right)$, the sign of $J(k, M)$ depends on M. By the definitions of M_1^c and M_2^c, we have proven that $I_M \neq \emptyset$. For $M \in I_M$, there exists at least one $k > 0$ such that $f(k, d) < g(k, M)$, i.e., $J(k, M) < 0$. For $M \in (M_1^c, M_2^c) \setminus I_M$, then for any $k > 0$, we have $f(k, d) > g(k, M)$, namely, $J(k, M) > 0$.

However, For $M > M_2^c$, we have $g(k, M) < f(k, d)$ for any $k > 0$ and both curves can not interact, which implies $J(k, M) > 0$. The conclusion (III) is confirmed. □

Remark 2.7 When $0 < d < d^{(1)}$, it is enough complicated to determine the sign of $J(k, M)$ explicitly for $M \in (M_1^c, M_2^c)$ since it depends on the values of M and d (which is dependent on the parameters a_{11}, a_{12}, a_2 and a_3). What is sure, however, is that when $d^{(3)} < d < d^{(1)}$, we have $I_M = (M_1^c, M_2^c)$, which means there exists $I_k \subset \mathbb{R}^+$ such that $J(k, M) < 0$ for $k \in I_k$ and $J(k, M) > 0$ for $k \notin I_k$ affirmatively for $M \in (M_1^c, M_2^c)$. We will describe and illustrate this situation after giving specific values by numerical simulation in Sect. 3.

When $a_{11} > 0$, we have $\min\limits_{k>0}\{f(k, d)\} \leq \max\limits_{k>0}\{g(k, M)\}$. For fixed d, it is easy to conclude that when $\min\limits_{k>0}\{f(k, d)\} \leq 0$, there must be an interval of k such that $f(k, d)$ is smaller than $g(k, M)$ when M is sufficiently large to M_3^c in which

$$M_3^c = \min_{M > M_1^c} \{M \,|\exists j \in \mathbb{N} \; s.t. \; g(k_c, M) > f(k_c, d) \quad and \; z_{2j} < k_c M < z_{2(j+1)}\Big\}, \tag{2.36}$$

where $k_c = \sqrt[4]{\frac{-a_2 a_3}{d}}$. Similar to the Lemma 2.6, we have the following results.

Lemma 2.8 *Assume that the conditions (C_0), (C_1) and (C_2) hold, $d^{(1)}$, $\tilde{d}$, I_M, M_1^c, M_2^c and M_3^c are defined by (2.27), (2.31), (2.35), (2.34) and (2.36), respectively. For $a_{11} > 0$, we have the following results:*

(I) *if $d > d^{(1)}$, $J(k, M) > 0$ for any $M > 0$ and $k > 0$;*

(II) *if $d = d^{(1)}$, $J(k_c, \frac{z_1}{k_c}) = 0$ and $J(k, M) > 0$ for $M \neq \frac{z_1}{k_c}$ where $k_c = \sqrt[4]{\frac{-a_2 a_3}{d}}$;*

(III) *if $\tilde{d} < d < d^{(1)}$, there exist two critical values M_1^c and M_2^c of M such that*

   (i) *for $M \in (0, M_1^c) \cup (M_2^c, +\infty)$, $J(k, M) > 0$ for $k > 0$;*
   (ii) *for $M = M_j^c$, $J(k_j^c, M_j^c) = 0$ and $J(k, M_j^c) > 0$ for $k \neq k_j^c (j = 1, 2)$;*
   (iii) *for $M \in (M_1^c, M_2^c)$, the sign of $J(k, M)$ depends on the value of M. More specifically, for $M \in I_M$, there exists at least $k > 0$ such that $J(k, M) < 0$; for $M \in (M_1^c, M_2^c) \setminus I_M$, then $J(k, M) > 0$ for any $k > 0$;*

(IV) *if $d^{(2)} < d \leq \tilde{d}$, there exist two critical values M_1^c and M_3^c of M such that*

   (i) *for $M \in \left(0, M_1^c\right)$, $J(k, M) > 0$ for $k > 0$;*
   (ii) *for $M = M_1^c$, $J(k_1^c, M_1^c) = 0$ and $J(k, M_1^c) > 0$ for $k \neq k_1^c$;*
   (iii) *for $M \in \left(M_1^c, M_3^c\right]$, the sign of $J(k, M)$ depends on the value M;*
   (iv) *for $M \in (M_3^c, +\infty)$, there exists $I_k \subset \mathbb{R}^+$ such that $J(k, M) < 0$ for $k \in I_k$ and $J(k, M) > 0$ for $k \notin I_k$;*

(V) *if $0 < d \leq d^{(2)}$, there exists a critical value M_1^c of M such that*

   (i) *for $M \in (0, M_1^c)$, $J(k, M) > 0$ for $k > 0$;*
   (ii) *for $M = M_1^c$, $J(k_1^c, M_1^c) = 0$ and $J(k, M_1^c) > 0$ for $k \neq k_1^c$;*
   (iii) *for $M \in (M_1^c, +\infty)$, there exists $I_k \subset \mathbb{R}^+$ such that $J(k, M) < 0$ for $k \in I_k$ and $J(k, M) > 0$ for $k \notin I_k$.*

Proof For $d > \tilde{d}$, it follows from (2.31) that we obtain $\min\limits_{k>0}\{f(k, d)\} > 0$. Thus the processes of proof (I)–(III) are similar to the proof of lemma 2.6.

For $0 < d \leq \tilde{d}$, it is easy to obtain $-1 < \min\limits_{k>0}\{f(k, d)\} \leq 0$ from (2.29) and (2.31). Analogously, when M is sufficiently small ($M < M_1^c$), $J(k, M) > 0$ for any $k > 0$.

When M varies from small to large to M_1^c, the curve $g = g(k, M_1^c)$ is firstly tangent to the curve $f = f(k, d)$ at $k = k_1^c$ and $f(k, d) > g(k, M_1^c)$ for $k \neq k_1^c$, which means $J(k_1^c, M_1^c) = 0$ and for $k \neq k_1^c$, we have $J(k, M_1^c) > 0$.

For $M > M_1^c$, the sign of $J(k, M)$ is more complicated, depending on the values of d and M. For $d \in (d^{(2)}, \tilde{d})$, more specifically, for $d \in \left(d^{(2j)}, d^{(2(j+1))}\right)$ ($j \in \mathbb{N}$), we have $\min_{k>0}\{f(k,d)\} \in \left(-\frac{\sin z_{2j}}{z_{2j}}, -\frac{\sin z_{2(j+1)}}{z_{2(j+1)}}\right)$. Notice that $\min_{k>0}\{f(k,d)\} = f(k_c, d)$ from (2.29) in which $k_c = \sqrt[4]{\frac{-a_2a_3}{d}}$, thus there exist the interval of M such that $f(k_c, d) < g(k_c, M)$ and $z_{2i} < k_c M < z_{2(i+1)}$. We define the the minimum value of M as M_3^c (defined by (2.36)). Thus for $M > M_3^c$, there must exist the interval $I_k \subset \mathbb{R}^+$ of k such that $f(k, d) < g(k, M)$, i.e. $J(k, M) < 0$ for $k \in I_k$. And for $M \in \left(M_1^c, M_3^c\right)$, the sign of $J(k, M)$ is complicated.

However, for $d \in \left(0, d^{(2)}\right]$, we have $\min_{k>0}\{f(k,d)\} \in \left(-1, -\frac{\sin z_2}{z_2}\right)$. For $M > M_1^c$, the minimum of $f(k, d)$ is always less than the local minimum of $g(k, M)$, which means there exist the interval $I_k \subset \mathbb{R}^+$ of k such that $f(k, d) < g(k, M)$, i.e. $J(k, M) < 0$ for $k \in I_k$. □

In addition, we have the following transversality conditions for Hopf bifurcation and Turing bifurcation. Taking M as the bifurcation parameter and letting $\lambda(M) = \mathrm{Re}\lambda(M) \pm i\mathrm{Im}\lambda(M)$ be the root of Eq. (2.10) satisfying $\mathrm{Re}\lambda(M_H) = 0, \mathrm{Im}\lambda(M_H) = \omega(\omega > 0)$, where M_H is defined by (2.23) for $k = k_H$, it follows from (2.10) and (2.11) that

$$\mathrm{Re}\left(\frac{\mathrm{d}\lambda(M)}{\mathrm{d}M}\right) = \frac{1}{2}\frac{\mathrm{d}T(k,M)}{\mathrm{d}M} = \frac{a_{12}}{2}\left(\frac{\cos(kM)}{M} - \frac{\sin(kM)}{kM^2}\right),$$

in which $0 < k_H M_H < z_1$. By (2.23), we have

$$\mathrm{Re}\left(\frac{\mathrm{d}\lambda(M)}{\mathrm{d}M}\right)\Bigg|_{k=k_H, M=M_H} = \frac{(d+1)k_H^2}{M_H} > 0.$$

Together with

$$\frac{\mathrm{dRe}\lambda(M)}{\mathrm{d}M} = \mathrm{Re}\left(\frac{\mathrm{d}\lambda(M)}{\mathrm{d}M}\right),$$

we have

$$\frac{\mathrm{dRe}\lambda(M)}{\mathrm{d}M}\Bigg|_{k=k_H, M=M_H} > 0. \tag{2.37}$$

Similarly, letting $\lambda(M)$ be the root of Eq. (2.10) satisfying $\lambda(M_1^c) = 0$ where M_1^c is defined by (2.34) for $k = k_1^c$, it follows from (2.10) and (2.11) that

$$\frac{\mathrm{d}\lambda(M)}{\mathrm{d}M} = \frac{1}{T(k,M)}\frac{\mathrm{d}J(k,M)}{\mathrm{d}M} = -\frac{a_{12}k^2}{T(k,M)}\left(\frac{\cos(kM)}{M} - \frac{\sin(kM)}{kM^2}\right),$$

in which $0 < k_1^c M_1^c < z_1$. By (2.33), we have $T(k_1^c, M_1^c) \neq 0$ if $k_1^c \neq k_H$, $M_1^c \neq M_H$ and

$$\frac{\mathrm{d}\lambda(M)}{\mathrm{d}M}\Bigg|_{k=k_1^c, M=M_1^c} \neq 0 \tag{2.38}$$

for $k_1^c M_1^c \neq z_1$.

Then combined with (2.37) and (2.38) and Lemmas 2.3, 2.5, 2.6, 2.8, we have the following results on the stability and bifurcation analysis of E_* for system (1.5), mainly investigating the influence of the perceptual radius M and the random diffusion coefficient d on the stability and bifurcations. All possible scenarios of the pattern formation are demonstrated as shown in Fig. 2.

Theorem 2.9 *Assume that the conditions* (C_0), (C_1) *and* (C_2) *hold and* $a_{12} \geq \beta a_{11}$. *For system* (1.5), *the steady state* E_* *is always asymptotically stable for any* $d > 0$ *and* $M > 0$.

Proof Based on the Lemmas 2.3 and 2.5, when $a_{12} \geq \beta a_{11}$, we have $T(k, M) < 0$ and $J(k, M) > 0$ for any $k > 0$ and $M > 0$, which implies that E_* is asymptotically stable. □

Theorem 2.10 *Assume that the conditions* (C_0), (C_1) *and* (C_2) *hold and* $a_{12} < \beta a_{11}$. $d^{(1)}$, M_H, M_1^c *are defined by* (2.27), (2.23) *and* (2.34), *respectively. For system* (1.5), *we have the following results:*

(I) *when* $d > d^{(1)}$, *the steady state* E_* *is asymptotically stable for* $M \in (0, M_H)$ *and unstable for* $M \in (M_H, +\infty)$, *and system* (1.5) *undergoes Hopf bifurcation at* $M = M_H$;
(II) *when* $0 < d \leq d^{(1)}$, *then we have the following results:*
  (i) *When* $M_H < M_1^c$, *the steady state* E_* *is asymptotically stable for* $M \in (0, M_H)$ *and unstable for* $M \in (M_H, +\infty)$, *and system* (1.5) *undergoes Hopf bifurcation at* $M = M_H$;
  (ii) *When* $M_H = M_1^c$, *the steady state* E_* *is asymptotically stable for* $M \in (0, M_H)$ *and unstable for* $M \in (M_H, +\infty)$, *and system* (1.5) *undergoes* $B - T$ *bifurcation at* $M = M_H$ *for* $k_H = k_1^c$ *and undergoes Turing–Hopf bifurcation at* $M = M_H$ *for* $k_H \neq k_1^c$;
  (iii) *When* $M_H > M_1^c$, *the steady state* E_* *is asymptotically stable for* $M \in \left(0, M_1^c\right)$ *and unstable*

for $M \in (M_H, +\infty)$ and system (1.5) undergoes Turing bifurcation at $M = M_1^c$, then for $M \in \left(M_1^c, M_H\right)$, stability switches may occur. Moreover, the stability of the steady state E_* is more complicated, E_* may be either stable for some subintervals of $\left(M_1^c, M_H\right)$ or unstable for other subintervals of $\left(M_1^c, M_H\right)$.

Proof When $a_{11} > -\frac{sin(z_1)}{z_1} a_{12}$, based on the Lemma 2.3, for $M \in (M_H, +\infty)$, $\exists\ I_k \subset \mathbb{R}^+$ such that $T(k, M) > 0$ for $k \in I_k$, which means E_* is unstable. From Lemmas 2.3, 2.6 and 2.8, we can conclude that when $d > d^{(1)}$, we have $J(k, M) > 0$ and $T(k, M) < 0$ for $M \in (0, M_H)$, which implies that the steady state E_* is asymptotically stable $M \in (0, M_H)$ and unstable for $M \in (M_H, +\infty)$. For $M = M_H$, we have $T(k_H, M_H) = 0$ and $J(k, M_H) > 0$ for any $k > 0$, which means system (1.5) undergoes Hopf bifurcation at $M = M_H$. The conclusion (I) is confirmed.

When $0 < d \le d^{(1)}$, from Lemmas 2.3, 2.6 and 2.8, we have E_* is asymptotically stable for $M \in (0, M^*)$ where $M^* = \min_M\{M_1^c, M_H\}$ and unstable for $M \in (M_H, +\infty)$. When $M^* = M_1^c$, the stability of E_* is more complicated, which may either unstable for some subintervals of (M^*, M_H), or stable for other subintervals of (M^*, M_H).

More specifically, for $M_H < M_1^c$, we have E_* is asymptotically stable for $M \in (0, M_H)$ and unstable for $M \in (M_H, +\infty)$. For $M = M_H$, it is easy to obtain that $T(k_H, M_H) = 0$ and $J(k, M_H) > 0$ for any $k > 0$, which means system (1.5) undergoes Hopf bifurcation at $M = M_H$ (see Fig. 2a–c, f).

For $M_H = M_1^c$, if there exists $k_1^c = k_H$ such that $T(k_1^c, M_H) = 0$, $J(k_H, M_H) = 0$, system (1.5) can undergo B-T bifurcation at $M = M_H$. If $k_1^c \neq k_H$, system (1.5) can undergo Turing–Hopf bifurcation at $M = M_H$ (see Fig. 2e).

For $M_H > M_1^c$, we have E_* is asymptotically stable for $M \in \left(0, M_1^c\right)$ and unstable for $M \in (M_H, +\infty)$. However, the stability of the steady state E_* is more complicated for $M \in \left(M_1^c, M_H\right)$, E_* may be either stable for some subintervals of $\left(M_1^c, M_H\right)$ or unstable for other subintervals of $\left(M_1^c, M_H\right)$ (see Fig. 2g–i). For $M = M_1^c$, we have $J(k_1^c, M_1^c) = 0$ and $T(k, M_1^c) < 0$ for any $k > 0$, which means system (1.5) undergoes Turing bifurcation at $M = M_1^c$ (see Fig. 2d). Figure 3 shows the real part of the eigenvalues of linear operator for the nine cases shown in Fig. 2. The conclusion (II) is confirmed. □

Remark 2.11 Under the hypothesis of Theorem 2.10, when we further analyze the case of (II)–(iii) (i.e.,$d \in \left(0, d^{(1)}\right]$ and $M_H > M_1^c$), there exist the critical values $(M_i^c, i = 2, 3)$ of M, so that we can have a deeper understanding of the stability (or instability) region. Then

(1) for $a_{11} \le 0$, there exists a critical value M_2^c defined by (2.34), then for any $d \in (0, d^{(1)})$,

(a) when $M_1^c < M_H < M_2^c$, system (1.5) undergoes Turing bifurcation at $M = M_1^c$;
(b) when $M_2^c = M_H$, system (1.5) could not undergo B-T bifurcation but Turing–Hopf bifurcation at $M = M_H$;
(c) when $M_H > M_2^c$, through analysis, we have E_* is also stable for $M \in (M_2^c, M_H)$, but ambiguous for $M \in (M_1^c, M_2^c)$. System (1.5) undergoes Hopf bifurcation at $M = M_H$ and Turing bifurcation at $M = M_j^c$ $(j = 1, 2)$.

(2) for $a_{11} > 0$, there exist critical values M_2^c and M_3^c defined by (2.34) and (2.36),respectively. Then we have:

(I) for $\tilde{d} < d \le d^{(1)}$, stability and branching analysis are the same as when $a_{11} \le 0$;
(II) for $0 < d \le \tilde{d}$, there exists a critical value M_3^c defined by (2.36), then

(a) when $M_1^c < M_H < M_3^c$, system (1.5) undergoes Turing bifurcation at $M = M_1^c$;
(b) when $M_3^c = M_H$, system (1.5) undergoes Turing–Hopf bifurcation at $M = M_H$;
(c) when $M_H > M_3^c$, we have E_* becomes unstable for $M \in (M_3^c, M_H)$, but not clear for $M \in (M_1^c, M_3^c)$. System (1.5) undergoes Turing bifurcation at $M = M_j^c$ $(j = 1, 3)$.

2.2 Stability and bifurcations for the case of $a_4 < 0$

After analyzing the stability and branching analysis when $a_4 = 0$, it will be possible to proceed to discuss the case of $a_4 < 0$. However, it is necessary for us to re-examine the conditions (C_0), (C_1) and (C_2) in this case. When $a_1 \le 0$, it is straightforward to obtain

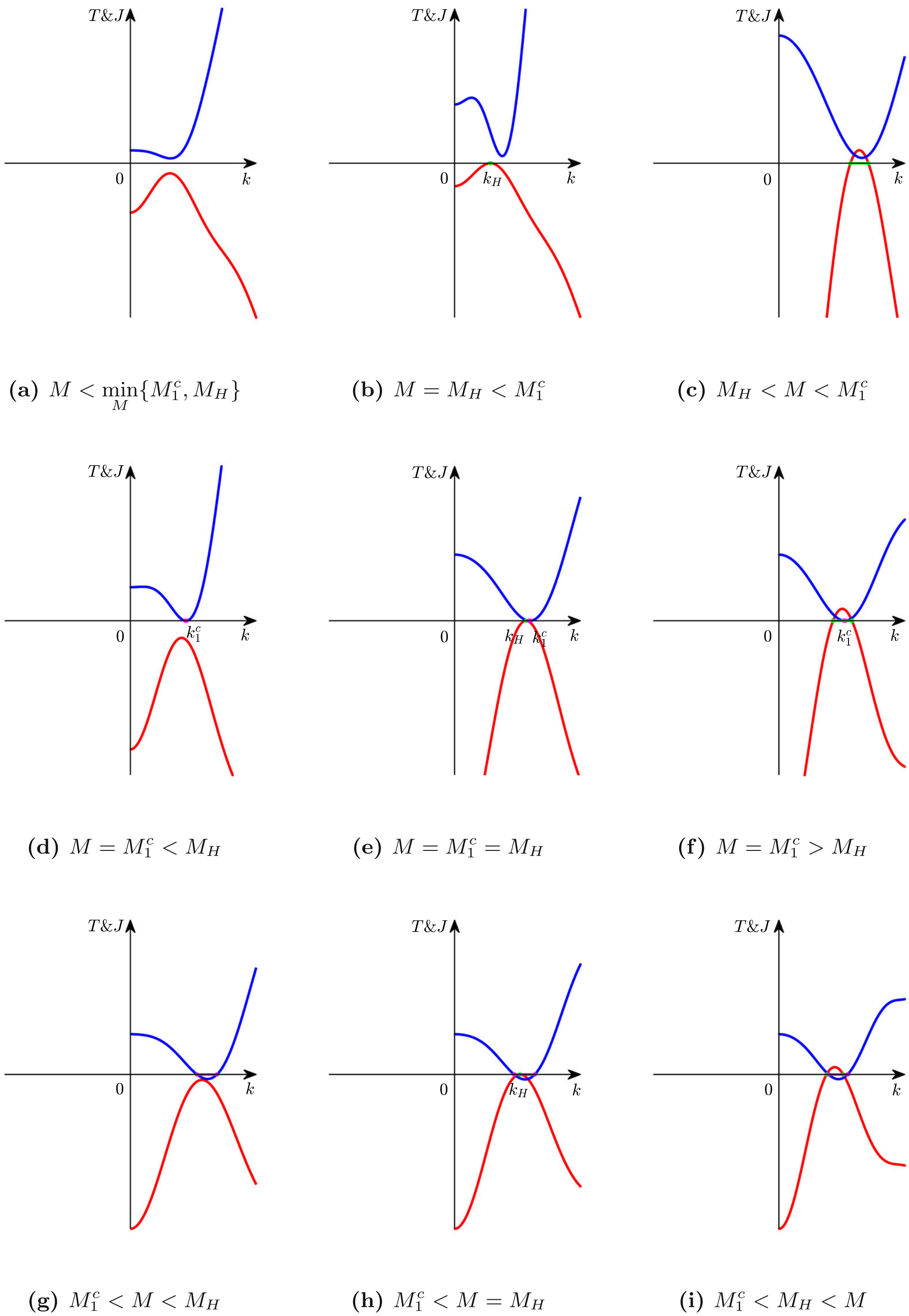

(a) $M < \min_M\{M_1^c, M_H\}$ **(b)** $M = M_H < M_1^c$ **(c)** $M_H < M < M_1^c$

(d) $M = M_1^c < M_H$ **(e)** $M = M_1^c = M_H$ **(f)** $M = M_1^c > M_H$

(g) $M_1^c < M < M_H$ **(h)** $M_1^c < M = M_H$ **(i)** $M_1^c < M_H < M$

Fig. 2 The demonstration for all possible scenarios of the pattern formation in system (1.5). In each figure, the red curve stands for $T(k, M)$ and the blue curve stands for $J(k, M)$ at fixed M

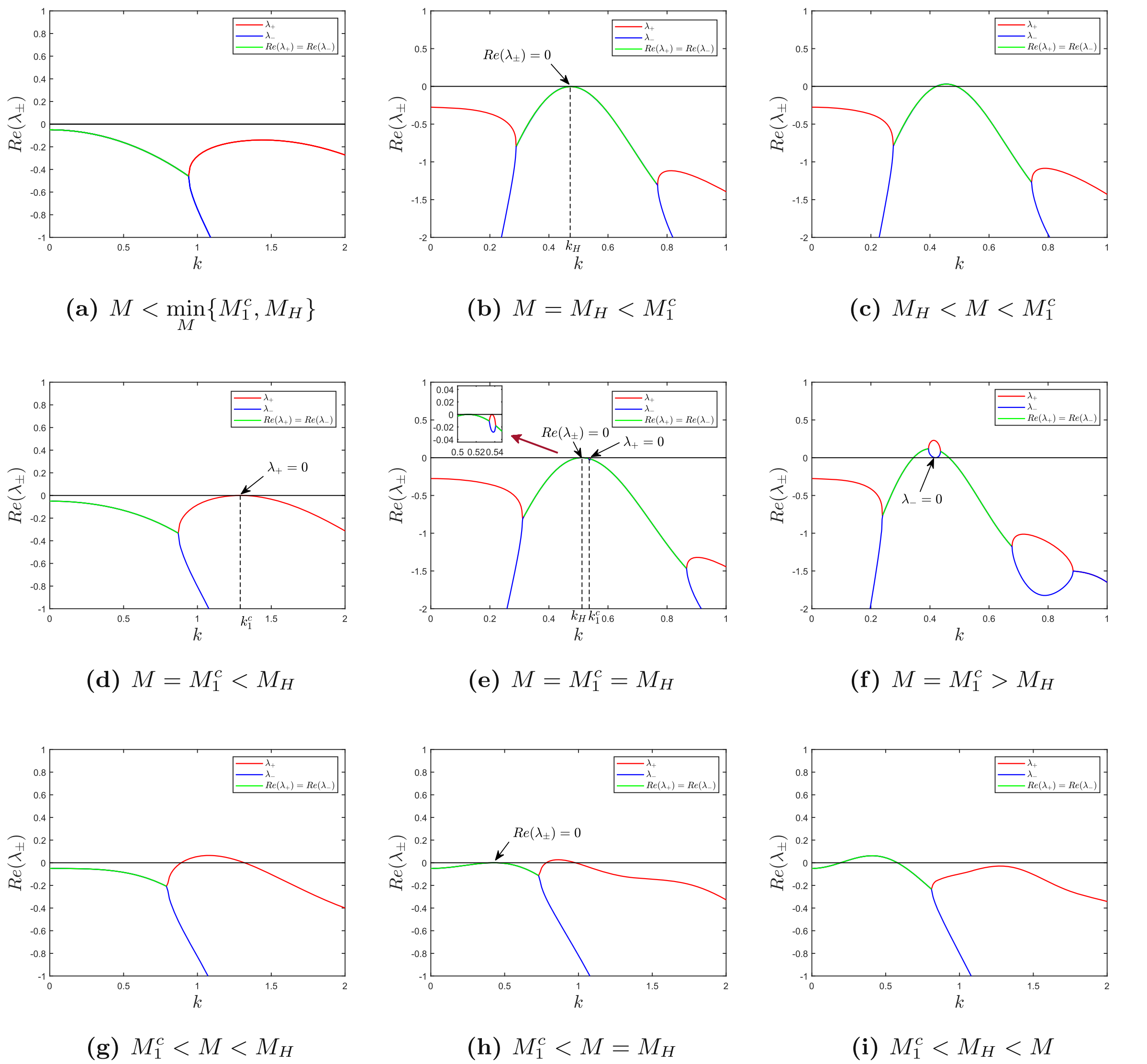

(a) $M < \min_M\{M_1^c, M_H\}$ (b) $M = M_H < M_1^c$ (c) $M_H < M < M_1^c$

(d) $M = M_1^c < M_H$ (e) $M = M_1^c = M_H$ (f) $M = M_1^c > M_H$

(g) $M_1^c < M < M_H$ (h) $M_1^c < M = M_H$ (i) $M_1^c < M_H < M$

Fig. 3 Roots of the dispersion relation for the linear operator (2.4) around E_*. For the characteristic equation (2.10), since $T(k, M)$ and $J(k, M)$ are independent of λ, then we have $\lambda_\pm = \frac{1}{2}\left(T(k, M) \pm \sqrt{T(k, M)^2 - 4J(k, M)}\right)$. In each figure, the red curve stands for the real number λ_+, the blue curve stands for the real number λ_- and the green curve stands for the real part of complex numbers $\lambda_\pm$ at fixed M. **a** All roots of Eq. (2.10) have negative real parts. **b** Equation (2.10) has a pair of purely imaginary roots when $M = M_H$, $k = k_H$. **d** Equation (2.10) has a zero root when $M = M_1^c$, $k = k_1^c$. **e** Shows that Eq. (2.10) has a pair of purely imaginary roots and a zero root when $M = M_1^c = M_H$. **c**, **f** and **g–i** There exist some k such that Eq. (2.10) has positive real roots or one pair of complex roots with positive real parts

that these conditions hold for any $a_4 < 0$. On the contrary, when $a_1 > 0$, we have the fact that the condition (C_0) holds if and only if

$$\frac{a_2a_3}{a_1} < a_4 < -a_1 \textit{ and } a_1^2 + a_2a_3 < 0.$$

In regard to the condition (C_1), it is equivalent to

$$\frac{a_1}{\sqrt{d}} + a_4\sqrt{d} < 2\sqrt{a_1a_4 - a_2a_3}.$$

Denoting $P(d) = \frac{a_1}{\sqrt{d}} + a_4\sqrt{d}$, we have $\frac{\mathrm{d}P(d)}{\mathrm{d}d} < 0$, $\lim_{d\to 0^+} P(d) = +\infty$ and $\lim_{d\to+\infty} P(d) = -\infty$ since $a_1 > 0$ and $a_4 < 0$. Hence there exists a critical d^* of d such that (C_1) holds for $d > d^*$ if we set

$$d^* = \frac{1}{a_4^2}\left(\sqrt{a_1a_4 - a_2a_3} - \sqrt{-a_2a_3}\right)^2. \tag{2.39}$$

Obviously, it follows from (2.28), (2.32) and (2.39) that we have

$$d^* < \tilde{d} < d_-^{(1)} < -\frac{a_2 a_3}{a_4^2},$$

since $0 < a_1 < a_{11} < a_{11} + \frac{\sin(z_1)}{z_1} a_{12}$. For the convenience of notation, we denote

$$d_c = \begin{cases} 0, & a_1 \le 0, \\ d^*, & a_1 > 0. \end{cases} \tag{2.40}$$

Then similarly to the case of $a_4 = 0$, depending on whether a_{12} is larger than βa_{11} or not, the discussion is divided into two cases. We firstly analyse the case of $a_{12} \ge \beta a_{11}$. Resembling Theorem 2.9, we have the following results.

Theorem 2.12 *Assume that the conditions* (C_0), (C_1) *and* (C_2) *hold and* $a_{12} \ge \beta a_{11}$. *For system* (1.5), *the steady state* E_* *is always asymptotically stable for any* $d > 0$ *and* $M > 0$.

Proof From Lemma 2.3, for $a_{12} \ge \beta a_{11}$, we have $a_1 < 0$ and $a_{12} \ge \beta a_{11} > \beta a_{11} + \beta a_4$, thus we have $T(k, M) < 0$ for any $k > 0$ and $M > 0$. From (2.30), for any $d > 0$, we have

$$\begin{aligned} \min_{k>0}\{f(k,d)\} &\ge \min_{k>0}\{f(k,0)\} = \frac{a_{11}}{a_{12}} \\ &\ge -\frac{sin(z_1)}{z_1} \ge \max_{k>0}\{g(k,M)\}, \end{aligned}$$

which means $f(k, d) > g(k, M)$, i.e., $J(k, M) > 0$ for any $k > 0$ and $M > 0$. □

For the case of $a_{12} < \beta a_{11}$, one shall take the sign of $J(k, M), T(k, M)$ into account as before. As for the former, it follows form (2.19) that when $f(0, d) = \frac{a_{11}a_4 - a_2 a_3}{a_{12} a_4} \le \max_{k>0}\{g(k, M)\}$ (equivalent to $a_4 \le \frac{-a_2 a_3 \beta}{a_{12} - \beta a_{11}}$), there merely exists a critical value M_1^c of M such that $J(k, M) > 0$ for $M \in \left(0, M_1^c\right)$ and for $M > M_1^c$, there exists $I_k \subset \mathbb{R}^+$ such that $J(k, M) < 0$ for $k \in I_k$ and $J(k, M) > 0$ for $k \notin I_k$. On the contrary, when $f(0, d) > \max_{k>0}\{g(k, M)\}$, the sign of $J(k, M)$ is analogous to the case of $a_4 = 0$.

On the other hand, from Lemma 2.3, we have $T(k, M) < 0$ for any $k > 0$ and $M > 0$ when $a_4 \le \frac{1}{\beta}(a_{12} - \beta a_{11})$. Thus the steady state E_* of system (1.5) can not be destabilized through the occurrence of Hopf bifurcation. When $a_4 > \frac{1}{\beta}(a_{12} - \beta a_{11})$, bifurcations such as Turing bifurcation, Hopf bifurcation and even Turing–Hopf bifurcation can be observed. We will analyze the specific model through numerical simulation in Sect. 3. Combining with the above-mentioned analysis, we obtain the following results similar to Theorem 2.10.

Theorem 2.13 *Assume that the conditions* (C_0), (C_1) *and* (C_2) *hold and* $a_{12} < \beta a_{11}$. d_c, $d_-^{(1)}$, M_1^c *and* M_H *are defined by* (2.40), (2.28), (2.34) *and* (2.23), *respectively. For system* (1.5), *we have the following results:*

(I) *For* $a_4 \le \frac{-a_2 a_3 \beta}{a_{12} - \beta a_{11}}$, *then for* $d > d_c$, *we have*

- (i) *when* $a_4 \le \frac{1}{\beta}(a_{12} - \beta a_{11})$, *the steady state* E_* *is always asymptotically stable for* $M \in \left(0, M_1^c\right)$ *and unstable for* $M \in \left(M_1^c, +\infty\right)$ *and system* (1.5) *undergoes Turing bifurcation at* $M = M_1^c$;
- (ii) *when* $\frac{1}{\beta}(a_{12} - \beta a_{11}) < a_4 < 0$, *the steady state* E_* *is always asymptotically stable for* $M \in (0, M^*)$ *and unstable for* $M \in (M^*, +\infty)$ *where* $M^* = \min_M\{M_1^c, M_H\}$;
  - (a) *when* $M^* = M_1^c$, *system* (1.5) *undergoes Turing bifurcation at* $M = M^*$;
  - (b) *when* $M^* = M_H$, *system* (1.5) *undergoes Hopf bifurcation at* $M = M^*$;
  - (c) *when* $M_1^c = M_H$, *system* (1.5) *undergoes Turing–Hopf bifurcation at* $M = M^*$ *for* $k_H \ne k_1^c$ *and* $B - T$ *bifurcation at* $M = M^*$ *for* $k_H = k_1^c$.

(II) *For* $\frac{-a_2 a_3 \beta}{a_{12} - \beta a_{11}} < a_4 < 0$, *similar to the case of* $a_4 = 0$,

- (i) *for* $d > d_-^{(1)}$, *then we have*
  - (a) *when* $a_4 \le \frac{1}{\beta}(a_{12} - \beta a_{11})$, *the steady state* E_* *is always asymptotically stable;*
  - (b) *when* $\frac{1}{\beta}(a_{12} - \beta a_{11}) < a_4 < 0$, *the steady state* E_* *is always asymptotically stable for* $M \in (0, M_H)$ *and unstable for* $M \in (M_H, +\infty)$ *and system* (1.5) *undergoes Hopf bifurcation at* $M = M_H$;
- (ii) *for* $d_c < d \le d_-^{(1)}$, *stability and bifurcation analysis resemble the case of* $a_4 = 0$.

3 Example and numerical simulations

In this section, based on the assumption that the intraspecific competition of prey is nonlocal, we consider the diffusive predator–prey models with Holling type-II functional response and illustrate the possible pattern formations induced by the the perceptual radius M, mainly considering diffusive Rosenzweig–MacArthur model and Lotka–Volterra model with the top-hat kernel function.

3.1 A diffusive Rosenzweig–MacArthur model with the top-hat kernel function ($a_4 = 0$)

For the sake of simplicity, we consider the following classical Rosenzweig–MacArthur model with nonlocal prey competition in the finite spatial domain $[-L, L]$ subject to periodic boundary conditions, which are convenient to extend the spatial domain to infinite domain and conducive to numerical simulation. The periodic boundary conditions are often used in the literature on cognitive animal locomotion models [13,33].

$$\begin{cases} u_t = du_{xx} + u(1 - K_M * u) - \dfrac{\alpha_1 uv}{\alpha_2 + u}, & -L < x < L, t > 0, \\ v_t = v_{xx} + \dfrac{\alpha_1 uv}{\alpha_2 + u} - \delta v, & -L < x < L, t > 0, \\ u(-L,t) = u(L,t),\ u_x(-L,t) = u_x(L,t), & t > 0, \\ v(-L,t) = v(L,t),\ v_x(-L,t) = v_x(L,t), & t > 0, \end{cases} \tag{3.1}$$

where K_M is top-hat kernel function defined by (1.2). The corresponding local version of model (3.1) was firstly established in [21]. Here, we analyse and discuss the nonlocal model (3.1) which is proposed in [3,17]. In [3], the analytical conditions for the emergence of spatially non-homogeneous stationary solutions of this model with the top-hat kernel were illustrated. In [17], the same model (3.1) was demonstrated by three different types of kernel functions, among which the top-hat kernel (Caution: it was named uniform kernel in [17]) with large standard deviation is conducive to the formation of spatiotemporal patterns. However, rigorous mathematical analyses and proofs can not be found. Therefore, on the strength of our theoretical results in Sect. 2, we reconsider this nonlocal model and show that the perceptual radius M can induce the possible pattern formations through bifurcations.

Let $E_* = (u_*, v_*)$ be the positive spatially homogeneous steady state of system (3.1), thus it is easy to obtain that

$$u_* = \frac{\alpha_2\delta}{\alpha_1 - \alpha_2}, \quad v_* = \frac{(1-u_*)(\alpha_2 + u_*)}{\alpha_1}$$

provided that $\alpha_1 > \delta(\alpha_2 + 1)$ and

$$\begin{aligned} &a_1 = -u_* + \tfrac{\alpha_1 u_* v_*}{(\alpha_2+u_*)^2} \begin{cases} < 0, & \alpha_2 > \frac{\alpha_1-\delta}{\alpha_1+\delta}, \\ \geq 0, & \alpha_2 \leq \frac{\alpha_1-\delta}{\alpha_1+\delta}, \end{cases} \\ &a_{11} = \tfrac{\alpha_1 u_* v_*}{(\alpha_2+u_*)^2} > 0,\ a_{12} = -u_* < 0, a_2 = -\tfrac{\alpha_1 u_*}{\alpha_2+u_*} < 0, \\ &a_3 = \tfrac{\alpha_1\alpha_2 v_*}{(\alpha_2+u_*)^2} > 0,\ a_4 = 0. \end{aligned} \tag{3.2}$$

From (3.2), it is easy to see that the condition (C_2) holds. Meanwhile, when $\alpha_2 > \frac{\alpha_1-\delta}{\alpha_1+\delta}$ (equivalent to $a_1 < 0$), the conditions (C_0) and (C_1) are satisfied since $a_4 = 0$. Then we take the parameters as follows:

$$\alpha_1 = 1.2,\ \alpha_2 = 0.4,\ \delta = 0.6.$$

Then we have $E_* = (0.4, 0.4)$ and

$$a_{11} = 0.3,\ a_{12} = -0.4,\ a_1 = -0.1,$$
$$a_2 = -0.6,\ a_3 = 0.3,\ a_4 = 0.$$

By Proposition 2.2, it is easy to see that the zeros z_j of the equation $tan(z) = z$ are

$$z_1 = 4.4934, z_2 = 7.7252, z_3 = 10.9041,$$
$$z_4 = 14.0662, z_5 = 17.2208,$$

and by $g_1(z_i) = -\frac{sin(z_j)}{z_j}(j \in \mathbb{N})$, we have

$$g_1(z_1) = 0.2172, g_1(z_2) = -0.1284, g_1(z_3) = 0.0913,$$

then by (2.27), we have

$$d^{(1)} = 0.2079,\ d^{(2)} = 0.08587,\ d^{(3)} = 0.1573,$$
$$\tilde{d} = 0.125.$$

For the numerical simulation, we choose $L = 50$ and consider the following initial conditions

$$u(x,0) = \begin{cases} 0.4, & |x| < 50, \\ 0, & \text{elsewhere}, \end{cases} \quad v(x,0) = \begin{cases} 0.4, & |x| < 50, \\ 0, & \text{elsewhere}. \end{cases} \tag{3.3}$$

With the choice of parameters, we have $a_{11} > -\frac{\sin(z_1)}{z_1}a_{12}$. In terms of Theorem 2.10, the Turing bifurcation curves $M = M_1^c$ and $M = M_2^c$ and Hopf bifurcation curves $M = M_H$ can be diagrammed in the $d - M$ plane as shown in Fig. 4. The shaded region is the stable region.

For $d^{(3)} < d = 0.2 < d^{(1)}$, we have the critical values of M, which are $M_1^c = 4.0352$, $M_2^c = 5.2655$, $M_H = 6.0591$. The positive steady state E_* is asymptotically stable for $M \in (0, M_1^c) \cup (M_2^c, M_H)$ and becomes unstable with emergence spatio-temporal patterns for $M \in (M_1^c, M_2^c) \cup (M_H, +\infty)$. For the point P_1 locating in the stable region, the positive constant equilibrium E_* is asymptotically stable for $M = 2 < M_1^c$,

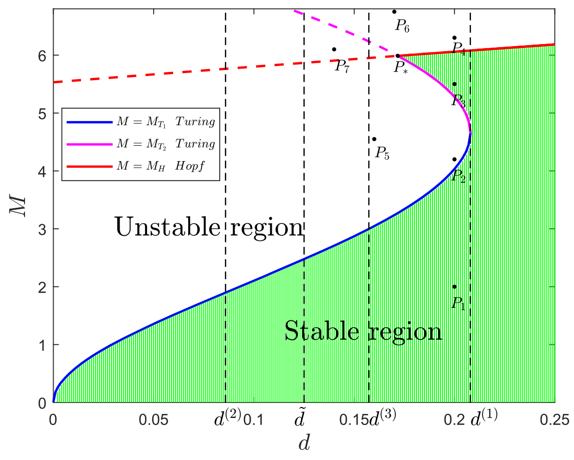

Fig. 4 Stability region and bifurcation diagrams in plane $d - M$ of system (3.1) with the top-hat kernel. With the choice of parameters, we have $d^{(1)} \doteq 0.2079$, $d^{(2)} \doteq 0.08587$, $d^{(3)} \doteq 0.1573$, $\tilde{d} \doteq 0.125$. The shaded region is the stable region for the positive constant steady state E_* of Eq. (3.1) while the blank area is unstable region. The Turing bifurcation curves are $M = M_{T_1}$ and $M = M_{T_2}$. Meanwhile, the Hopf bifurcation curve is $M = M_H$

as shown in Fig. 5a, e. With the increasing the of M, we can observe the vertical strip patterns at $M = 4.2 > M_1^c$, as shown in Fig. 5b, f. For the point P_3 crossing Turing bifurcation line $M = M_2^c$ and locating in the stable region, the positive constant equilibrium E_* is asymptotically stable again for $M = 5.5 \in (M_2^c, M_H)$, as shown in Fig. 5c, g. Figure 5d, h illustrate the spatially inhomogeneous periodic solution emerges with spot patterns at $M = 6.3 > M_H$ for P_4.

In the neighbourhood of the Turing–Hopf bifurcation point $P_* \doteq (0.1717, 5.9873)$, we observed the Turing–Hopf patterns that appeared in the form of spots and stripes. For the point P_5, it falls in the unstable region below P_*, Fig. 6a, d show the existence of dots and strips mixed pattern. Among them, there are stripes in the middle and dots on both sides. For the point of P_6 in the unstable region above P_*, Fig. 6b, e show the existence of a inverted V-shaped spot-stripe pattern. More accurately, there are dots in the middle and diagonal stripes on both sides. For the point of P_7 in the unstable region on the left side of P_*, some irregular dot patterns are displayed in Fig. 6c, f, with the middle being relatively dark and sparse, while the sides are bright and dense.

3.2 A diffusive Lotka–Volterra model with the top-hat kernel function($a_4 < 0$)

Next we consider the diffusive Lotka–Volterra model with the top-hat kernel function and study the possible pattern formations induced by the perceptual radius M in the finite spatial domain$[-L, L]$ subject to periodic boundary conditions:

$$\begin{cases} u_t = du_{xx} + u\left(r_1 - aK_M * u - v\right), & -L < x < L, t > 0, \\ v_t = v_{xx} + v(-r_2 + u - bv), & -L < x < L, t > 0, \\ u(-L,t) = u(L,t), u_x(-L,t) = u_x(L,t), & t > 0, \\ v(-L,t) = v(L,t), v_x(-L,t) = v_x(L,t), & t > 0, \end{cases} \tag{3.4}$$

where K_M is top-hat kernel function defined by (1.2). For a biological explanation of the classical Lotka–Volterra model and further extension to stochastic case, see the monograph by Samanta [22]. Obviously, the positive equilibrium $E_* = (u_*, v_*)$ of system (3.4) is given by

$$u_* = \frac{r_2 + br_1}{1 + ab}, \quad v_* = \frac{r_1 - ar_2}{1 + ab}$$

with the assumption that $r_1 - ar_2 > 0$ and

$$\begin{aligned} &a_{11} = 0, a_{12} = -au_* < 0, a_1 = -au_* < 0, \\ &a_2 = -u_* < 0, a_3 = v_* > 0, \\ &a_4 = -bv_* < 0. \end{aligned}$$

Then for the numerical illustrations, we take the parameters as follow:

$$a = 2.2, b = 2, r_1 = 5, r_2 = 2,$$

then we find that $E_* = \left(\frac{20}{9}, \frac{1}{9}\right)$ and

$$\begin{aligned} &a_{11} = 0, \ a_{12} = -\frac{44}{9}, \ a_1 = -\frac{44}{9}, \\ &a_2 = -\frac{20}{9}, \ a_3 = \frac{1}{9}, \ a_4 = -\frac{2}{9}. \end{aligned}$$

It is easy to verify that the conditions (C_0), (C_1) and (C_2) are satisfied with the choice of above parameters for any $d > 0$ since $a_1 < 0$. Meanwhile, we have $a_4 > \frac{-a_2 a_3 \beta}{a_{12} - \beta a_{11}}$ and $a_4 > \frac{1}{\beta}(a_{12} - \beta a_{11})$. Hence by Theorem 2.13 (II) and (2.28), we conclude that for $d > d_-^{(1)} \doteq 3.1163$, we have E_* of system (3.4) is stable for $M < M_H$ and unstable for $M > M_H$, accompanied by the occurrence of Hopf bifurcation for $M = M_H$. For $0 < d \leq d_-^{(1)}$, similar to $a_4 = 0$, the Turing bifurcation curve $M = M_1^c$ and Hopf bifurcation curve $M = M_H$ can be diagrammed in the $d - M$ plane as shown in Fig. 7 and a spatially homogeneous

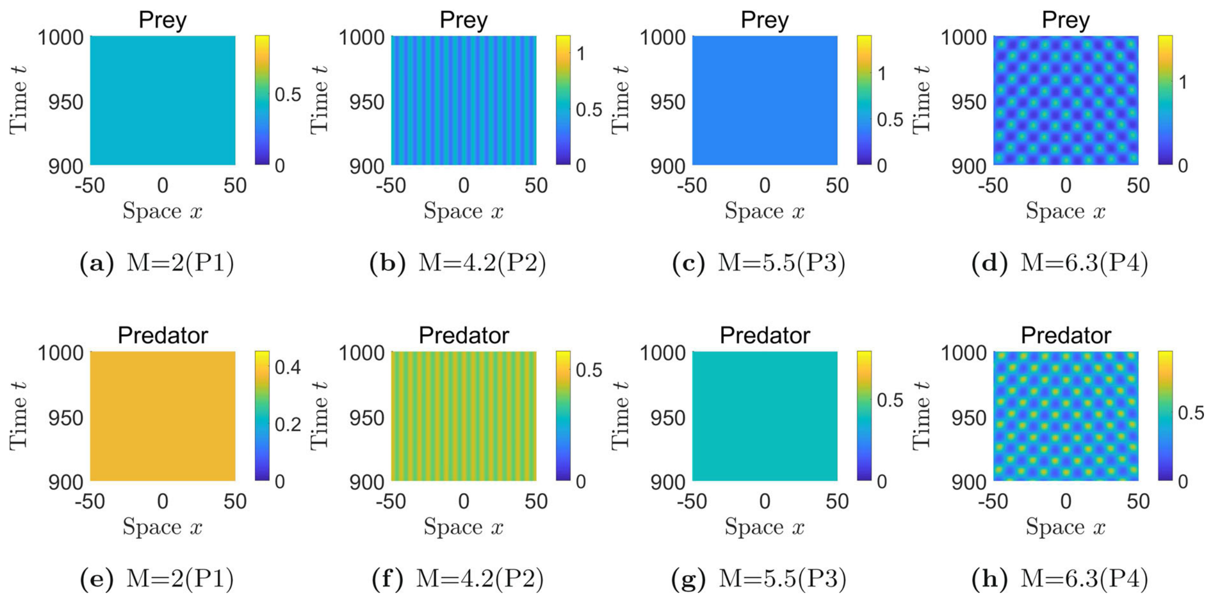

Fig. 5 Numerical simulations for different values M for system (3.1) with $d = 0.2 \in (d^{(3)}, d^{(1)})$. **a**, **e** E_* is asymptotically stable for $M = 2 < M_1^c$; **b**, **f** spatial nonhomogeneous steady state with the vertical strip patterns for $M = 4.2 > M_1^c = 4.0352$, **c**, **g** E_* is asymptotically stable for $M = 5.5 \in (M_2^c, M_H)$; **d**, **h** spatial nonhomogeneous periodic oscillation with spot patterns for $M = 6.3 > M_H = 6.0591$

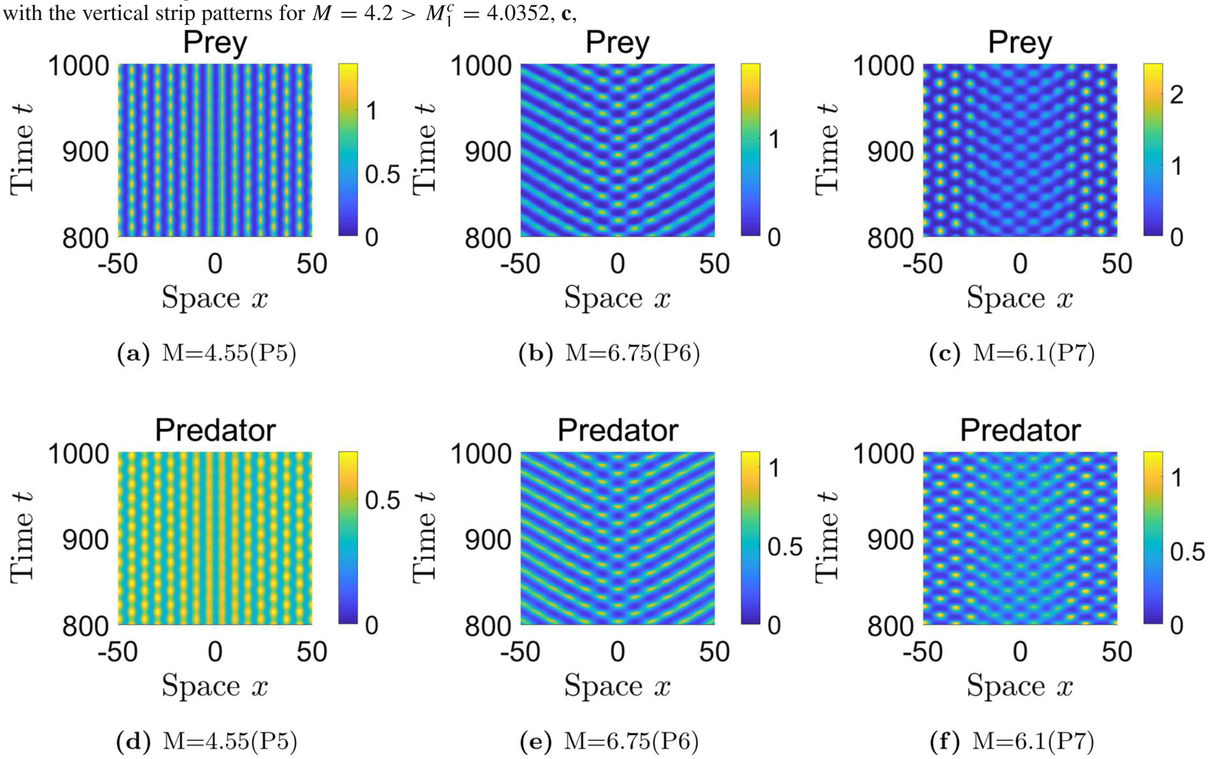

Fig. 6 Numerical simulations for different values M for system (3.1) in the neighbourhood of the Turing–Hopf bifurcation point $P_*(0.1717, 5.9873)$. There are critical values of M are $M_H = 5.95725$, $M_1^c = 3.0502$ and $M_2^c = 6.1866$. **a**, **d** The existence of dots and strips mixed patterns with stripes in the middle and dots on both sides for $P_5(0.16, 4.55)$; **b**, **e** the existence of a inverted V-shaped spot-stripe pattern with dots in the middle and diagonal stripes on both sides for $P_6(0.17, 6.75)$; **c**, **f** some irregular dot patterns with the middle being relatively dark and sparse, while the sides are bright and dense for $P_7(0.14, 6.1)$

steady state solution of (3.4) exists lying in the shaded region of $d-M$ plane. The positive constant steady state E_* of Eq. (3.4) is stable in the shaded region but unstable in the blank area.

For the numerical simulation, we choose $L=50$ and consider the following initial conditions:

$$u(x,0)=\begin{cases}\frac{20}{9}, & |x|<50,\\ 0, & \text{elsewhere},\end{cases}\quad v(x,0)=\begin{cases}\frac{1}{9}, & |x|<50,\\ 0, & \text{elsewhere}.\end{cases} \tag{3.5}$$

In the neighbourhood of the Turing–Hopf bifurcation point $P_*\doteq(1.977, 8.137)$, we observed four points $P_j(j=1,2,3,4)$ of different spatio-temporal dynamics. For $d=1.98$, we have the critical values $M_H=8.1405$ and $M_1^c=8.1481$. For the point $P_1(1.98, 6.5)$ lying in the stability region, the steady state E_* is asymptotically stable as shown in Fig. 8a, e. When M is increasing, the spot-stripe pattern can be observed in Fig. 8c, g at $P_3(1.98, 8.17)$. Figure 8b, f illustrate the spatially inhomogeneous periodic solution that present a pattern of spots for the point $P_2(2.2, 8.74)$. For the point $P_4(1.8, 7.7)$, Fig. 8d, h illustrate the Turing patterns at $M=7.7$ which is larger than and close to the Turing bifurcation value $M_1^c\doteq7.4362$.

4 Conclusion and discussion

In this paper, we investigate the spatiotemporal dynamics in a general nonlocal reaction–diffusion system with the top-hat kernel function. We are chiefly concerned with the influence of the diffusion coefficient d and the competition radius M of the prey on the stability of the positive constant steady state E_* and the possible bifurcation phenomena when $a_{12}<0$ and $a_4\le0$.

Under the basic assumptions that the positive constant steady state E_* is locally asymptotically stable for the system without nonlocal prey competition ($M=0$). Letting $\beta=-z_1/\sin(z_1)\doteq4.6033$, then in terms of the relationship between $a_{11}=\partial f(u, K*u, v)/\partial u$ and $a_{12}=\partial f(u, K*u, v)/\partial K*u$ evaluated at E_*, where $a_{12}<0$ measures the strength of the nonlocal prey competition, the main findings are summarized as follows:

(1) For $a_{12}\ge\beta a_{11}$, the nonlocal competition radius M does not affect the stability of the positive constant steady state E_*, which means E_* is always asymptotically stable for any $M>0$. This implies that when the strength of the nonlocal prey competition is weak, the size of the competition radius does not change the dynamics.

(2) For $a_{12}<\beta a_{11}$, the nonlocal competition radius M can affect the stability of E_*. In this case, the spatiotemporal dynamics depend not only on the nonlocal competition radius M but also on the diffusion coefficient d of the prey. More specifically, for the case of $a_4=0$, depending on whether the diffusion coefficient d of the prey is larger than a threshold value $d^{(1)}$ or not, there are two cases: (i) for $d>d^{(1)}$, there only exists Hopf bifurcation induced by the nonlocal competition radius such that E_* is asymptotically stable for $M\in(0, M_H)$ and unstable for $M\in(M_H, +\infty)$, and the system undergoes Hopf bifurcation at $M=M_H$. (ii) for $d<d^{(1)}$, E_* is asymptotically stable for M is smaller than some critical value $M^*=\min_M\{M_1^c, M_H\}$, and Turing bifurcation, Hopf bifurcation and Turing–Hopf bifurcation are possible for large competition radius. This implies that when the nonlocal prey competition is dominant, the joint of the nonlocal competition radius M and the diffusion coefficient d of the prey can lead to more complex dynamics.

Finally, employing the obtained theoretical results to the diffusive Rosenzweig–MacArthur and Lotka–Volterra models with nonlocal prey competition and taking d and M as the bifurcation parameters, the stability region and bifurcation curves can be completely determined in the $d-M$ plane. The spatial patterns with different spatial modes arising from the Turing bifurcation and oscillatory patterns with spatially inhomogeneous profiles are found. It has been shown that when the diffusion coefficient d of the prey is small, the positive constant steady state E_* loses its stability via Turing bifurcation with spatial patterns, when d is large, E_* loses its stability via Hopf bifurcation with oscillatory patterns. What's particularly interesting is that when d belongs to some appropriate interval, there exists stability switches induced by the nonlocal competition radius M, i.e., the positive constant steady state E_* undergoes changes from stability to instability to stability and finally to instability with the increasing of M.

Compared with previous literature [1,2,4,18] on the dynamics of the nonlocal prey competition with the top-

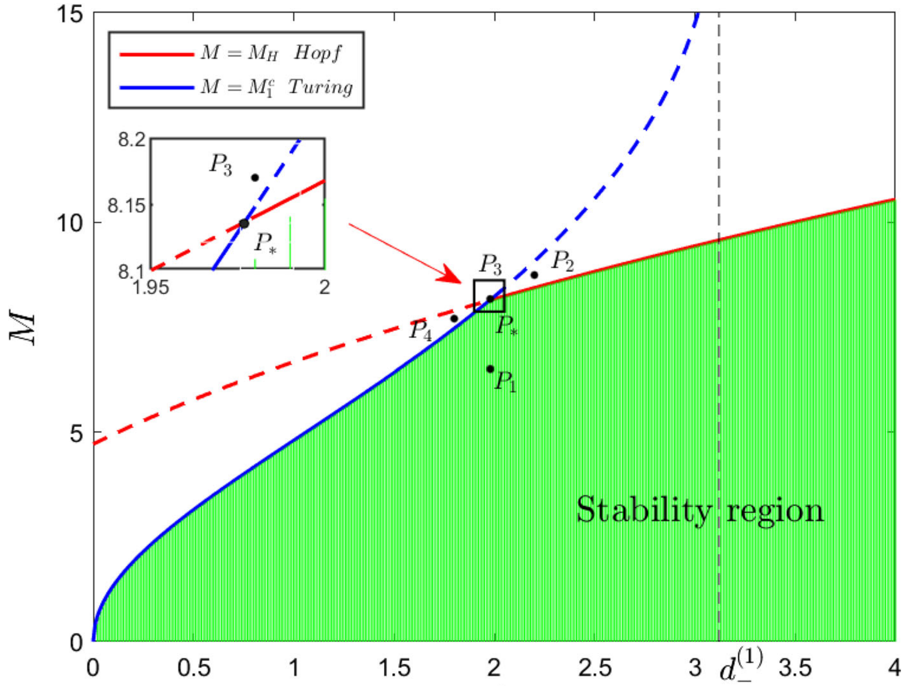

Fig. 7 Stability region and bifurcation diagrams in plane $d - M$ of system (3.1) with the top-hat kernel. The shaded region is the stability region. The Turing bifurcation curve is $M = M_1^c$. Meanwhile, the Hopf bifurcation curve is $M = M_H$. The inset is Turing–Hopf bifurcation point P_* locally enlarged view

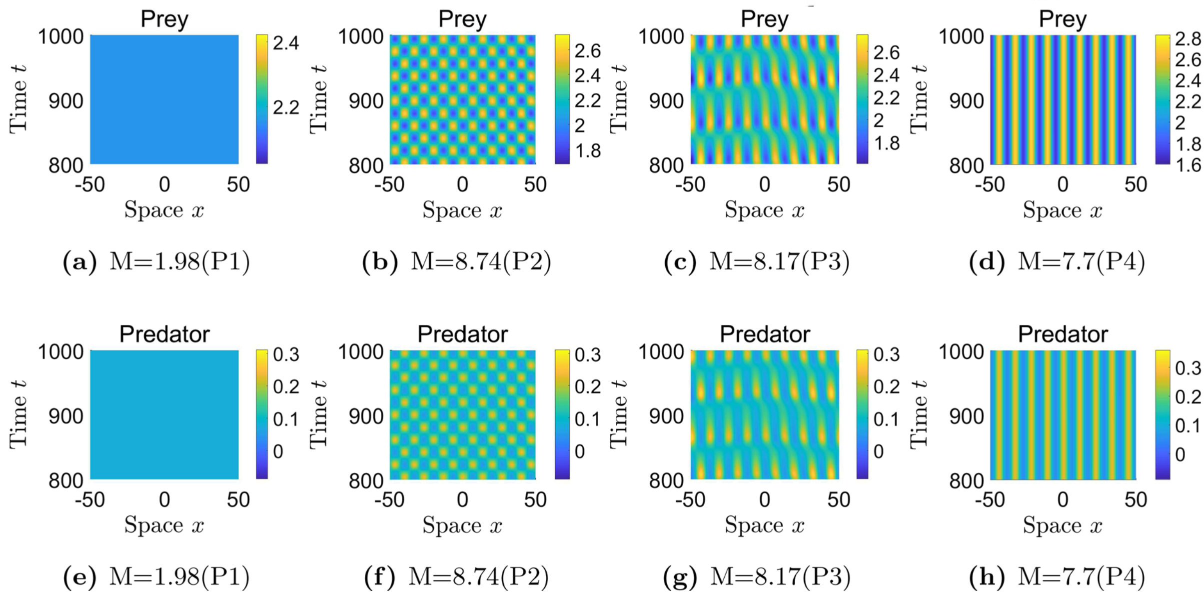

Fig. 8 Numerical simulations for different spatio-temporal patterns induced by the the perceptual radius M of system (3.4). We take into account the points $P_j (j = 1, 2, 3, 4)$ in the neighbourhood of Turing–Hopf bifurcation point $P_*(1.977, 8.137)$. **a**, **e** $P_1(1.98, 6.5)$; **b**, **f** $P_2(2.2, 8.74)$; **c**, **g** $P_3(1.98, 8.17)$; **d**, **h** $P_4(1.8, 7.7)$

hat functional response, the main advances contained in this paper are reflected in the following aspects:

- Stability and bifurcation analysis for a general non-local predator–prey system with the top-hat kernel function are investigated. The obtained results can be easily applied to many specific predator–prey models.
- The analytic conditions for the occurrences of the Turing bifurcation, Hopf bifurcation and Turing–Hopf bifurcation are completely determined via

taking the nonlocal competition radius M and the diffusion coefficient d of the prey.

- For the diffusive Rosenzweig–MacArthur and Lotka–Volterra models with nonlocal prey competitions, the stability region and bifurcation curves are completely determined in the $d - M$ plane.
- For the diffusive Rosenzweig–MacArthur model with nonlocal prey competitions, oscillatory patterns arising from the Hopf bifurcation and stability switches induced by the nonlocal competition radius M are observed.
- For the diffusive Rosenzweig–MacArthur and Lotka–Volterra models with nonlocal prey competitions, more types of spatiotemporal patterns near the Turing–Hopf bifurcation point are discovered.

We would also like to mention some further interesting investigations. Recently, the study on the memory-based diffusive movement has become a hot and important topic in the field of population dynamics [24,26,27,30]. It is worth incorporating memory-based diffusion into the nonlocal diffusive population models with the top-hat kernel function and investigating the joint effect of the nonlocal competition radius and the memory diffusion on the dynamics of the population model.

Acknowledgements The authors are grateful to the reviewer's valuable comments, which led to the improvement of this article.

Funding This work is partially supported by the grants from Natural Science Foundation of Zhejiang Province (No. LZ23A 010001) and National Natural Science Foundation of China (Nos. 12371166 and 12071105).

Data Availability Statement Not applicable. No datasets were generated or analyzed during the study.

Declarations

Conflict of interest The authors declare that they have no conflict of interest.

References

1. Banerjee, M., Kuznetsov, M., Udovenko, O., Volpert, V.: Nonlocal reaction–diffusion equations in biomedical applications. Acta. Biotheor. **70**(2), 1–28 (2022)
2. Banerjee, M., Mukherjee, N., Volpert, V.: Prey–predator model with a nonlocal bistable dynamics of prey. Mathematics **6**(3), 41 (2018)
3. Banerjee, M., Volpert, V.: Spatio-temporal pattern formation in Rosenzweig–Macarthur model: effect of nonlocal interactions. Ecol. Complex. **30**, 2–10 (2017)
4. Banerjee, M., Zhang, L.: Stabilizing role of nonlocal interaction on spatio-temporal pattern formation. Math. Model. Nat. Phenom. **11**(5), 103–118 (2016)
5. Chen, S., Yu, J.: Stability and bifurcation on predator–prey system with nonlocal prey competition. Discret. Contin. Dyn. Syst. **38**(1), 43–62 (2018)
6. Cintra, W., Molina-Becerra, M., Suarez, A.: The Lotka–Volterra models with non-local reaction terms. Commun. Pure Appl. Anal. **21**(11), 3865–3886 (2022)
7. Djilali, S.: Pattern formation of a diffusive predator-prey model with herd behavior and nonlocal prey competition. Math. Methods Appl. Sci. **43**(5), 2233–2250 (2020)
8. Fagan, W.F., Gurarie, E., Bewick, S., Howard, A., Cantrell, R.S., Cosner, C.: Perceptual ranges, information gathering, and foraging success in dynamic landscapes. Am. Nat. **189**(5), 474–489 (2017)
9. Furter, J., Grinfeld, M.: Local vs. non-local interactions in population dynamics. J. Math. Biol. **27**(1), 65–80 (1989)
10. Gao, J., Guo, S.: Patterns in a modified Leslie–Gower model with Beddington–DeAngelis functional response and nonlocal prey competition. Int. J. Bifurc. Chaos **30**(5), 2050074 (2020)
11. Geng, D., Jiang, W., Lou, Y., Wang, H.: Spatiotemporal patterns in a diffusive predator–prey system with nonlocal intraspecific prey competition. Stud. Appl. Math. **148**(1), 396–432 (2022)
12. Genieys, S., Volpert, V., Auger, P.: Pattern and waves for a model in population dynamics with nonlocal consumption of resources. Math. Model. Nat. Phenom. **1**(1), 63–80 (2006)
13. Giunta, V., Hillen, T., Lewis, M., Potts, J.R.: Local and global existence for nonlocal multispecies advection–diffusion models. SIAM J. Appl. Dyn. Syst. **21**(3), 1686–1708 (2022)
14. Jiang, J., Yu, P.: Multistable phenomena involving equilibria and periodic motions in predator–prey systems. Int. J. Bifurc. Chaos **27**(03), 1750043 (2017)
15. Liu, Y., Duan, D., Niu, B.: Spatiotemporal dynamics in a diffusive predator prey model with group defense and nonlocal competition. Appl. Math. Lett. **103**, 106175 (2020)
16. Manna, K., Volpert, V., Banerjee, M.: Pattern formation in a three-species cyclic competition model. Bull. Math. Biol. **83**(5), 52 (2021)
17. Merchant, S.M., Nagata, W.: Instabilities and spatiotemporal patterns behind predator invasions with nonlocal prey competition. Theor. Popul. Biol. **80**(4), 289–297 (2011)
18. Pal, S., Ghorai, S., Banerjee, M.: Analysis of a prey–predator model with non-local interaction in the prey population. Bull. Math. Biol. **80**(4), 906–925 (2018)
19. Pal, S., Ghorai, S., Banerjee, M.: Effect of kernels on spatio-temporal patterns of a non-local prey–predator model. Math. Biosci. **310**, 96–107 (2019)
20. Peng, Y., Zhang, G.: Dynamics analysis of a predator–prey model with herd behavior and nonlocal prey competition. Math. Comput. Simul. **170**, 366–378 (2020)
21. Rosenzweig, M.L., MacArthur, R.H.: Graphical representation and stability conditions of predator–prey interactions. Am. Nat. **97**(895), 209–223 (1963)
22. Samanta, G.: Deterministic, Stochastic and Thermodynamic Modelling of some Interacting Species. Springer, Berlin (2021)

23. Segal, B., Volpert, V., Bayliss, A.: Pattern formation in a model of competing populations with nonlocal interactions. Physica D **253**, 12–22 (2013)
24. Shen, H., Song, Y., Wang, H.: Bifurcations in a diffusive resource-consumer model with distributed memory. J. Differ. Equ. **347**, 170–211 (2023)
25. Shen, Z., Liu, Y., Wei, J.: Double Hopf bifurcation in nonlocal reaction-diffusion system with spatial average kernel. Discrete Contin. Dyn. Syst. Ser. B **28**(4), 2424–2462 (2022)
26. Shi, J., Wang, C., Wang, H.: Diffusive spatial movement with memory and maturation delays. Nonlinearity **32**(9), 3188–3208 (2019)
27. Shi, J., Wang, C., Wang, H., Yan, X.: Diffusive spatial movement with memory. J. Dyn. Differ. Equ. **32**(2), 979–1002 (2020)
28. Shi, Q., Shi, J., Song, Y.: Effect of spatial average on the spatiotemporal pattern formation of reaction–diffusion systems. J. Dyn. Differ. Equ. **34**(3), 2123–2156 (2022)
29. Shi, Q., Song, Y.: Spatiotemporal pattern formation in a pollen tube model with nonlocal effect and time delay. Chaos Solitons Fractals **165**(1), 112798 (2022)
30. Song, Y., Shi, J., Wang, H.: Spatiotemporal dynamics of a diffusive consumer-resource model with explicit spatial memory. Stud. Appl. Math. **148**(1), 373–395 (2022)
31. Song, Y., Shi, Q.: Stability and bifurcation analysis in a diffusive predator–prey model with delay and spatial average. Math. Methods Appl. Sci. **46**, 5561–5584 (2023)
32. Song, Y., Wang, H., Wang, J.: Cognitive consumer-resource dynamics with nonlocal perception. J. Nonlinear Sci. (2023) (in press)
33. Wang, H., Salmaniw, Y.: Open problems in pde models for knowledge-based animal movement via nonlocal perception and cognitive mapping. J. Math. Biol. **86**(5), 71 (2023)
34. Wu, S., Song, Y.: Stability and spatiotemporal dynamics in a diffusive predator–prey model with nonlocal prey competition. Nonlinear Anal. Real World Appl. **48**, 12–39 (2019)
35. Wu, S., Song, Y., Shi, Q.: Normal forms of double Hopf bifurcation for a reaction–diffusion system with delay and nonlocal spatial average and applications. Comput. Math. Appl. **119**, 174–192 (2022)
36. Yan, S., Jia, D., Zhang, T., Yuan, S.: Pattern dynamics in a diffusive predator–prey model with hunting cooperations. Chaos Solitons Fractals **130**, 109428 (2020)
37. Yang, R., Nie, C., Jin, D.: Spatiotemporal dynamics induced by nonlocal competition in a diffusive predator–prey system with habitat complexity. Nonlinear Dyn. **110**(1), 879–900 (2022)
38. Yang, R., Song, Q., An, Y.: Spatiotemporal dynamics in a predator–prey model with functional response increasing in both predator and prey densities. Mathematics **10**(1), 17 (2021)
39. Yang, R., Wang, F., Jin, D.: Spatially inhomogeneous bifurcating periodic solutions induced by nonlocal competition in a predator–prey system with additional food. Math. Methods Appl. Sci. **45**(16), 9967–9978 (2022)
40. Yuan, S., Xu, C., Zhang, T.: Spatial dynamics in a predator–prey model with herd behavior. Chaos **23**(3), 033102 (2013)